Transcriptional and Cellular Response of hiPSC-derived Microglia-Neural Progenitor Co-Cultures Exposed to IL-6

Amalie C. M. Couch[1,2*], Amelia Brown[1,2], Morgan Taylor[1], Laura Sichlinger[1,2], Rugile Matuleviciute[1,2], Deepak P. Srivastava[1,2§], Anthony C. Vernon[1,2*§].

1. Department of Basic and Clinical Neuroscience, Institute of Psychiatry, Psychology and Neuroscience, King's College London, London, UK.
2. MRC Centre for Neurodevelopmental Disorders, King's College London, London, UK.

§ These authors share joint senior authorship

***Joint Corresponding authors:**
Dr. Anthony Vernon and Dr. Amalie Couch
Department of Basic and Clinical Neuroscience
Maurice Wohl Clinical Neuroscience Institute
Institute of Psychiatry, Psychology and Neuroscience
King's College London
London SE5 9RT, United Kingdom

Tel: +44 (0) 207 848 5311
Email: anthony.vernon@kcl.ac.uk or amalie.c.couch@kcl.ac.uk

KEYWORDS
IL-6, neurodevelopment, human induced-pluripotent stem cells, microglia, neural progenitor cells.

Abstract

Elevated interleukin (IL-)6 levels during prenatal development have been linked to increased risk for neurodevelopmental disorders (NDD) in the offspring, but the mechanism remains unclear. Human-induced pluripotent stem cell (hiPSC) models offer a valuable tool to study the effects of IL-6 on features relevant for human neurodevelopment *in vitro*. We previously reported that hiPSC-derived microglia-like cells (MGLs) respond to IL-6, but neural progenitor cells (NPCs) in monoculture do not. We therefore investigated whether co-culturing hiPSC-derived MGLs with NPCs would trigger a cellular response to IL-6 stimulation via secreted factors from the MGLs. Using N=4 donor lines without psychiatric diagnosis, we first confirmed that NPCs can respond to IL-6 through trans-signalling when recombinant IL-6Ra is present, and that this response is dose-dependent. In response to IL-6, MGLs secreted soluble IL-6R, but at lower levels than found in vivo and below that needed to activate trans-signalling in NPCs. Among other cytokines, MGLs also increased Tumour necrosis factor (TNF)α secretion into the co-culture environment. Despite this, whilst transcriptomic analysis confirmed that MGLs undergo substantial transcriptomic changes after IL-6 exposure, NPCs in co-culture with MGLs exhibited a minimal transcriptional response. Furthermore, there were no significant cell fate-acquisition changes when differentiated into post-mitotic cultures, nor alterations in synaptic densities in mature neurons. These findings highlight the need to investigate if trans-IL-6 signalling to NPCs is a relevant disease mechanism linking prenatal IL-6 exposure to increased risk for psychiatric disorders. Moreover, our findings underscore the importance of establishing more complex *in vitro* human models with diverse cell types, which may show cell-specific responses to microglia-released cytokines to fully understand how IL-6 exposure may influence human neurodevelopment.

Introduction

Human birth cohort studies have linked elevated maternal interleukin (IL)-6 concentrations across gestation with aberrant structural and functional brain connectivity (as measured with MRI) in the offspring, which in turn are associated with abnormal cognitive development and increased risk for neurodevelopmental disorders (NDDs) such as autism spectrum condition (ASC) and schizophrenia (SZ) (Graham *et al.*, 2018; Rudolph *et al.*, 2018; Rasmussen *et al.*, 2019; Allswede *et al.*, 2020). Although these cohort studies demonstrate a correlation between elevated prenatal IL-6 and NDD incidence, additional studies at a molecular and cellular level are required to elucidate the molecular mechanisms by which this risk is conferred. Much of the cellular level research that links prenatal IL-6 insults with adverse neurodevelopmental effects in the offspring has however been conducted in rodent models (Samuelsson *et al.*, 2006; Smith *et al.*, 2007; Ozaki *et al.*, 2020; Mirabella *et al.*, 2021), which may have different brain development trajectories (Eze et al., 2021) For example, transient elevation of IL-6 during a critical period of neurodevelopment can have enduring effects on the formation of glutamatergic synapses in the mouse hippocampus with consequences for mouse brain connectivity as measured by resting state fMRI (Samuelsson *et al.*, 2006; Mirabella *et al.*, 2021). Nonetheless, investigating the influence of IL-6 on early neurodevelopmental processes using human-led models is crucial to understand its role in increasing the risk of NDDs in offspring (Bayés *et al.*, 2011; Südhof, 2017; Kuljis *et al.*, 2019).

As previously reviewed, IL-6 signalling involves both the IL-6 receptor (IL-6Ra) and IL-6 signal transducer (IL-6ST) subunits, with IL-6 binding to IL-6Ra triggering a conformational change that activates the JAK/STAT pathway through either cis-

signalling (cell surface IL-6Ra expression) or trans-signalling (via secreted soluble IL-6Ra, sIL-6Ra) (Rose-John, 2001, 2012, 2018; Wolf, Rose-John and Garbers, 2014). Trans-signalling via sIL-6Ra enables activation of cells lacking the full receptor and may be implicated in pro-inflammatory effects on non-glial cells, contrasting cis-signalling's proposed anti-inflammatory effects (Rose-John, 2001, 2012; Rose-John *et al.*, 2009; Scheller *et al.*, 2011; Campbell *et al.*, 2014; Wolf, Rose-John and Garbers, 2014). This mechanism is known to occur in the CNS, demonstrated when blocking trans-signalling with soluble IL-6ST in the CNS of adult rodents resulted in reduced astrogliosis and microgliosis, blood-brain barrier leakage, vascular proliferation, neurodegeneration, as well as impaired neurogenesis, that was caused by an overexpression of IL-6 (Campbell *et al.*, 2014). However, the consequences of trans-IL-6 signalling during human development remains unclear.

IL-6Ra is predominantly expressed and secreted by microglia in the developing human telencephalon (Nowakowski *et al.*, 2017) and to a lesser extent by astrocytes, but not neurons, in both foetal and adult brains (Zhang *et al.*, 2016; Couch *et al.*, 2023). The initiation of either IL-6 trans- or classic signalling may be dependent on the expression ratios of the receptor complex's subunits (Reeh *et al.*, 2019). However, the direct link between increased sIL-6Ra secretion by microglia and enhanced trans-signalling in non-glial cells (Ferreira *et al.*, 2013; Campbell *et al.*, 2014), and its implications in a neurodevelopment system remain uncertain, especially in a human-relevant model. This knowledge gap underscores the value of using human-induced pluripotent stem cells (hiPSCs) to model human foetal brain development (Eze *et al.*, 2021). While hiPSC-derived NPCs express IL-6ST, they lack the IL-6Ra subunit (Couch *et al.*, 2023; Sarieva, Hildebrand, *et al.*, 2023), rendering them unresponsive to IL-6 in mono-

culture without the addition of sIL-6Ra necessary for trans-signalling (Sarieva, Hildebrand, *et al.*, 2023). This limitation has been circumvented in previous *in vitro* studies by using hyper-IL-6, a synthetic construct combining sIL-6Ra and IL-6 linked by a flexible peptide, enabling NPCs to respond to IL-6 through trans-signalling (Sarieva, Hildebrand, *et al.*, 2023). Recent investigations using a 3D human forebrain organoid, which lacked microglia, demonstrated that exposure to hyper-IL-6 disproportionately affected radial glia cells, leading to an increased presence of this cell type in the organoid (Sarieva, Kagermeier, *et al.*, 2023). Notably, IL-6 exposure also resulted in an increase in upper-layer excitatory neurons and abnormalities in neuronal migration and positioning, suggesting that forced IL-6 trans-signalling can disrupt the standard process of cortical development and organization (Sarieva, Kagermeier, *et al.*, 2023). These data provide human-relevant evidence that IL-6 signalling in developing forebrain organoids can change typical cellular and molecular phenotypes.

Although hyper-IL-6 effectively demonstrates that NPCs are capable of IL-6 trans-signalling, it does not replicate the hypothesised physiological trans-signalling process found *in vivo,* since cells are forced to respond via trans-signalling under any condition when in reality there could be an upstream signalling regulation mechanism governed by non-NPC cell types. Our previous research indicates that hiPSC-derived microglia-like cells (MGLs) can secrete sIL-6Ra, addressing the absence of this subunit in hiPSC-derived NPCs (Couch *et al.*, 2023). Consequently, a co-culture system of MGLs and developing cortical NPCs may offer a more physiologically relevant model to study the acute IL-6 responses of both cell types, providing a closer approximation to physiological conditions than hyper-IL-6. In this study, we employ hiPSC-derived

MGLs and NPCs from the same donor for co-culture, ensuring a consistent genetic background within each culture, and expose them to acute IL-6 stimulation for 24 hours. Employing a trans-well co-culture system allows for the analysis of soluble factors versus direct contact, minimizing potential confounding impact from the experimental handling of microglia, and precludes the need for more invasive separation methods like fluorescence-activated cell sorting (FACS) (Park *et al.*, 2020). The overall study aim was to ascertain the cellular and molecular responses of both NPCs and MGLs post-IL-6 exposure. We hypothesised that: (1) co-culturing with MGLs will facilitate acute NPC response to IL-6 via trans-signalling mediated by sIL-6Ra, or additional cytokines secreted by MGLs in response to IL-6; (2) this interaction will modify the transcriptomes of both MGLs and NPCs, as identified through bulk RNAseq, revealing key molecular pathways; (3) early exposure of NPCs to cytokines will influence their cell fate determination and synaptogenesis upon differentiation into post-mitotic cortical neurons.

Methods

Cell Culture

hiPSCs: For the derivation of human induced pluripotent stem cells (hiPSCs), participants were recruited, and methods carried out in accordance with the 'Patient iPSCs for Neurodevelopmental Disorders (PiNDs) study' (REC No 13/LO/1218). Informed consent was obtained from all subjects for participation in the PiNDs study. Ethical approval for the PiNDs study was provided by the NHS Research Ethics Committee at the South London and Maudsley (SLaM) NHS R&D Office. Human iPSCs were generated and characterized from a total of four lines donated by three

males and one female with no history of neurodevelopmental or psychiatric disorders (Supplementary Table 1) the characteristics of which are previously described elsewhere (Warre-Cornish *et al.*, 2020; Adhya *et al.*, 2021; Couch *et al.*, 2023) and grown in hypoxic conditions on Geltrex™ (Life Technologies; A1413302) coated 6-well NUNC™ plates in StemFlex medium (Gibco, A3349401) exchanged every 48 hours. For passaging, cells were washed with HBSS (Invitrogen; 14170146) and then passaged by incubation with Versene (Lonza; BE17-711E), then plated in fresh StemFlex onto fresh Geltrex-coated 6-well NUNC™ plates.

Microglia-like and Neural Progenitor Cell Co-culture: Microglia-like cells (MGL) differentiation from hiPSCs was performed following a previously published protocol (van Wilgenburg *et al.*, 2013; Haenseler *et al.*, 2017), and successfully replicated by our group (Couch *et al.*, 2023). Simultaneously but in separate cultures, hiPSCs from the same lines were neuralised towards neural progenitor cells (NPCs) using a modified dual SMAD inhibition protocol to develop a mixture of excitatory and inhibitory forebrain neuronal subtypes (Shi, Kirwan and Livesey, 2012; Warre-Cornish *et al.*, 2020; Adhya *et al.*, 2021; Bhat *et al.*, 2022; Couch *et al.*, 2023). MGL progenitors were seeded directly from the embryoid body factory onto 0.4 µm Transparent PET Membrane Permeable Support Cell Culture Inserts (Falcon®; 353090) and allowed to differentiate for 12 days, after which they were assembled on top of the NPCs that had been differentiating in parallel for 16 days (Supplementary Figure 1). This permitted the NPCs to settle after neural passaging the day before on day 15 of their differentiation. Both cell types were then cultured together for 48h in co-culture media (1X N2 supplement, 2mM Glutamax, 100ng/ml IL-34 and 10ng/ml GM-CSF), to allow the two cell types to “equilibrate”. Specifically, during their initial optimization trials for

establishing the hiPSC to MGL differentiation method, Haenseler *et al.* (2017) raised concerns regarding the presence of corticosterone, superoxide dismutase, and catalase compounds in the B27 supplement. Therefore, B27 was removed from co-culture medium to guarantee compatibility with iPSC-derived cortical neurons while preserving microglial function (Haenseler *et al.*, 2017). The co-cultures were then exposed to 100ng/ml IL-6 or vehicle control (sterile water with 100 pM acetic acid) in fresh media, for 24h (Supplementary Figure 1). This meant stimulation on the microglial differentiation day 14, and neural progenitor differentiation day 18 (Couch *et al.*, 2023). The differentiation timepoints and 100ng/ml IL-6 dosage were based on previously published data that examined the IL-6 dose-response in day 14 MGLs (Couch *et al.*, 2023). After 24h of IL-6 or vehicle exposure, MGLs and NPCs were reseparated. All MGLs were collected for RNAseq, half NPCs were collected for RNAseq, and half were terminally differentiated into post-mitotic neurons as follows (Supplementary Figure 1).

Post-mitotic Cortical Neuron Differentiation: After 24h of IL-6 stimulation in co-culture with MGLs, half the NPCs were subsequently terminally differentiated into post-mitotic cortical neurons. Briefly, NPCs to be terminally differentiated were passaged on three days after IL-6 stimulation (D21) into 50ng/ml poly-l-ornithine (Gibco; A3890401) and 20ng/ml laminin (Sigma; L2020) coated 96-well Perkin Elmer CellCarrier Ultra plates, at a density of 100,000 cells/well in 1X B27 + 10µM DAPT + 10µM Rock inhibitor and incubated (37°C; 5% CO_2; 20% O_2). After 24 hours, medium was replaced with Rock inhibitor-free medium every 24 hours until D28. After this time frame, the notch inhibitor DAPT was removed from the medium as continued half medium exchanges every 7 days with 1X B27 only occurred.

sIL6Ra ELISA

The IL-6 Receptor (Soluble) Human ELISA Kit (Invitrogen; BMS214) was used to quantify soluble IL-6Ra expression in cell culture media, following the manufacturer's instructions. Media was collected from cultures and immediately centrifuged (300 x *g* for 2min) to remove cells in suspension, used undiluted and measured in duplicate on the ELISA plate to provide technical replicates. The optical density (OD) of the microwells was blanked and measured at 450nm. The sIL6Ra concentration was estimated against a seven-point reference curve.

Cytokine Profiler

Media was taken from cells in co-culture and immediately spun at 300 x *g* for 2 minutes to remove cells and cellular debris from the supernatant, which was transferred to a new tube, snap frozen and stored at -80ºC until use. Co-culture media samples were grouped and pooled by treatment condition, leaving two membranes to be stained with either vehicle or IL-6 treated culture supernatant. Cytokine profiling was carried out following the manufactures instructions using the Proteome Profiler Human XL Cytokine Array Kit **(**R&D Systems; ARY022B). The kit contained membranes with dots of 105 different immobilised cytokine antibodies dotted with two technical replicates each (Supplementary Figure 5). Each membrane was imaged for 10 minutes using the Bio-Rad Molecular Imager® Gel Doc™ XR System. Dot blot signals were quantified using the Protein Array Analyzer Palette plug-in for ImageJ, and technical dot replicates averaged to one value. These values were then corrected for background staining by subtracting the mean negative reference value from each of the signals. Each corrected value was then normalized by dividing by the mean positive reference value on the membrane.

Custom *Meso Scale Discovery Cytokine Array*

Based on the previous cytokine profiler analysis, the concentrations of MIP-1a, TNF-α, IL-8, and VEGF-A in vehicle/IL-6 treated co-culture, plus 24h treated NPC and MGL monoculture media (N = 3 healthy male donors M3_CTR, 014_CTM and 127_CTM) was measured using a custom U-Plex Biomarker Group 1 (Human) Multiplex Assay (K15067M-1, Meso Scale Discovery), following the manufacturer's instructions. Antibodies for each of the four analytes were cross-linked to a unique spot in each well of a 96-well plate. Each sample was incubated for 2 hours on the plate in technical triplicate, in addition to a seven-point standard curve. A secondary detection antibody was then added and incubated for 2 hours. The plate was read on an MESO QuickPlex SQ 120MM Imager, and data was obtained using Discovery Workbench 4.0 (Meso Scale Discovery).

RNA extraction, RNA Library Preparation and NovaSeq Sequencing

RNA extraction: In total, N=4 donors (Supplementary Table 1) were differentiated for co-culture IL-6 treatment, providing a total of 8 samples for downstream bulk RNA sequencing (RNAseq) analysis. Cells cultured for RNA extraction were collected at RT in TRI Reagent™ Solution (Invitrogen; AM9738) by splashing the cells with TRI Reagent™ Solution using a p1000, after removing media and stored at -80ºC. 1ml of TRI Reagent™ Solution per 6-well was used for NPCs, and 0.5ml of TRI Reagent™ Solution per 6-well was used for MGLs. RNA was extracted from each sample by centrifugation with 200µl of 100% Chloroform (10,000 x *g* for 5 minutes at 4ºC). The top aqueous layer was moved to a new 1.5ml tube with 500µl of 100% isopropanol and mixed 10 times by inversion and incubated 15 minutes at RT. Then, RNA was precipitated by centrifugation (17,000 x *g*, 15 minutes at 4ºC). The supernatant was

removed, and the pellet was washed in 1ml of 80% ethanol followed by centrifugation (20,000 x *g*, 5 minutes at 4ºC). The ethanol was then removed, the pellet air dried for 15 minutes at RT and then dissolved in 30µl of nuclease free water. Precipitation of RNA by 0.3M Sodium-acetate and 100% ethanol at -80ºC overnight was done to clean samples further, before an additional 80% ethanol wash and subsequent resuspension in 30µl RNAse-free water. Nucleic acid content was measured using NanoDrop™ One.

Library Preparation and NovaSeq Sequencing: Total RNA was submitted for sequencing at Genewiz Inc (South Plainfield, NJ). The following library reparations and RNA sequencing was carried out by Genewiz. Libraries were prepared using a polyA selection method using the NEBNext Ultra II RNA Library Prep Kit for Illumina following manufacturer's instructions (NEB, Ipswich, MA, USA) and quantified using Qubit 4.0 Fluorometer (Life Technologies, Carlsbad, CA, USA). RNA integrity was checked with RNA Kit on Agilent 5300 Fragment Analyzer (Agilent Technologies, Palo Alto, CA, USA). The sequencing libraries were multiplexed and loaded on the flowcell on the Illumina NovaSeq 6000 instrument according to manufacturer's instructions. The samples were sequenced using a 2x150 Pair-End configuration v1.5. Image analysis and base calling were conducted by the NovaSeq Control Software v1.7 on the NovaSeq instrument.

Upon receipt of FASTQ files from Genewiz, the subsequent bioinformatic analysis were performed. Files were quality controlled using Fastqc (Wingett and Andrews, 2018) and aligned to the human reference genome (GRCh38) with STAR (Dobin *et*

al., 2013), then sorted and duplicates removed with samtools version 1.13 (Li *et al.*, 2009) and Picard version 2.26.2 respectively, all within the King's CREATE high performance computing systems (King's College London, 2022). Downstream gene expression analyses were carried out in R version 4.0.2 (R Core Team, 2020). A count table was prepared and filtered for counts ≥ 1 using featureCounts (Liao *et al.*, 2014) from the Rsubread (Liao, Smyth and Shi, 2019) package, version 2.4.3. Differential gene expression analysis was carried out using DESeq2 (Love, Huber and Anders, 2014) version 1.30.1 and the default Wald test. Subsequently, using the Benjamini-Hochberg (BH) method, only genes with adjusted $p < 0.05$ were considered differentially expressed and submitted for downstream analyses.

Over-Representation and MGEnrichment Analyses

Over representation analysis (ORA) was carried out using WebGestalt (Liao *et al.*, 2019), where differentially expressed genes were tested for over representation of non-redundant cellular component, biological process and molecular function gene ontology terms. This analysis used as a background list all genes considered expressed in our model, according to DESeq2s's internal filtering criteria (i.e., adjusted $p \neq NA$). Enrichment p-values were corrected for multiple testing using the BH method, and only terms with adjusted $p < 0.05$ were considered significant. To understand the similarity of the microglial gene sets generated to those from other publications, the MGEnrichment tool was used (Jao and Ciernia, 2021). Genes that were either up- or down- regulated (adjusted $p < 0.05$) were imputed into the tool, backgrounded as above. Only human enrichment were selected, and modules were considered significant with an adjusted $p < 0.05$ after BH multiple testing correction.

Immunocytochemistry

On day 50 of neural differentiation, 29 days after seeding at a density of 30,000 cells/well into 96-well Perkin Elmer CellCarrier Ultra plates, cells were fixed and stained for immunocytochemistry (ICC). Briefly, cells were fixed with 4% paraformaldehyde (w/v; made in 4% sucrose PBS) for 20 min at room temperature. Samples were then washed twice in PBS, then simultaneously permeabilized and blocked with 2% normalised goat serum (NGS) PBS + 0.1 % Triton X-100 for 2 hours at RT. All antibodies (Supplementary Table 2) were diluted in 2% NGS in PBS. Primary antibodies were incubated with cells overnight at 4ºC, and secondary antibodies were incubated with cells for 1 hour at RT, both in humidified chambers. Between incubations, cells were washed three times in PBS at 15 min intervals. Finally, cells were incubated for 10 min in PBS + DAPI (1:50,000). After the final DAPI stain, cells were left in 150µl/well PBS ready for imaging on an OperaPhenix high throughput imaging system (Perkin Elmer) using a 20x water objective over 10 consistent fields of view per well. Overall, there were 4 technical repeat wells per staining condition on each plate, coupled with 2 primary-negative wells and 2 secondary-negative wells.

Cell-Marker Expression Assay: Cortical neurons were ICC stained with DAPI and β-tubulin III (TUBB3, antibody name TUJ1) to identify morphological boundaries, alongside glial fibrillary acidic protein (GFAP) and paired box protein (Pax6) to identify astrocytes and undifferentiated cortical NPCs respectively (Supplementary Table 2). Using the DAPI stain for PAX6 given it's expected expression in the nucleus, and TUJ1 stain for GFAP given it's expected expression in the cytoplasm, the number of cells positive for each marker per well was defined by the intensity of marker being above the background, which was calculated from the lowest intensity limit of each channel's

background florescence (mean 5 random locations from the primary negative wells). The number of PAX6+, MAP2+ and TUJ1+ cells per well were collated, and relative populations within each donor were calculated as a percentage of total cells counted.

Synapse Counting Assay: In order to identify nuclei and neurite sections on which synapses lie in cortical neurons, DAPI and MAP2 staining was performed respectively (Nieland *et al.*, 2014). In addition, a combination of specific pre- and post-synaptic proteins was utilized for staining, including the pre-synaptic protein, vesicular glutamate transporter 1 (vGlut1) and post-synaptic protein, postsynaptic density protein 95 (PSD95), or Synaptic vesicle glycoprotein 2A (SV2A, pre-synaptic) and the N-methyl-D-aspartate receptor subunit GluN1(post-synaptic) (Supplementary Table 2). Furthermore, the staining also involved a combination of inhibitory synaptic proteins, Gephyrin (post-synaptic) and glutamate decarboxylase (GAD67; pre-synaptic) (Supplementary Table 2) (Shum *et al.*, 2015, 2020; Deans *et al.*, 2017). The following assay analysis was carried out using an automatic script, applied to all replicate wells across donor plates using the Harmony software (Perkin Elemer), with an average of 1400 cells/donor. Initially, MAP2+ cells were identified (Supplementary Figure 3). Then, dendrites were automatically identified using the MAP2+ cell masks, using a software-integrated algorithm (http://www.csiro.au) (Supplementary Figure 3). Along each dendrite, pre- and post-synaptic puncta were then identified separately from either the 568nm or 488nm imaging channel depending on the secondary antibodies used. Synaptic puncta were thresholded by two characteristics: size and intensity. Synaptic puncta sizes were considered to be between 27-170 pixels, which equated to between 0.8-5μm^2 (Glynn and McAllister, 2006). To calculate the lowest intensity limit, the intensity of each channel's background fluorescence was taken and averaged from 5

random locations from the primary negative wells. To identify maximum intensity, fluorescence intensity from 5 clear artefacts in the primary negative wells were averaged. The dendrite length of MAP2+ cells was measured and averaged per well, to normalise the number of puncta for culture and dendrite outgrowth. This gave two outputs for each puncta channel: intensity and puncta number/dendrite length (density) (Supplementary Figure 3). Finally, positively identified puncta were masked on top of each other, to count those that co-colocalised (50% positively overlapped). For each donor, synaptic puncta metrics were averaged from all replicate images for each condition. To reduce the possibility of confounding results caused by staining differences across donor replicate plates, all IL-6 treated puncta metrics were normalised to the vehicle average to create a fold change value from vehicle within donor.

Statistical Analysis

All statistical analyses were conducted using Prism 9 for macOS version 9.3.1 (GraphPad Software LLC, California, USA), except for the RNAseq analyses which were carried out using the research computing facility at King's College London, CREATE, along with R version 4.0.2 (R Core Team, 2020). Each specific test performed is described in the corresponding figure legend and supplementary statistical data table, providing the number of replicate hiPSC lines included in each technical and biological replicate, as specified in the relevant method section above. In general, when discussion co-culture data, the N=4 donors (Supplementary Table 1) were considered biological replicates, and when discussing mono-culture data the N=3 donors (3 ♂ only, Supplementary Table 1) were considered biological replicates. To compare post-mitotic cell marker populations, two-way ANOVA was used with both

variables being cell type and treatment condition. When assessing the effect of IL-6 on each synaptic metric measured in post-mitotic neurons, one-sample Welch's t-test was used due to the unequal variances between each group on fold-change values from the vehicle-treated condition (all vehicle donor points = 1). To compare the concentrations of cytokines and sIL-6Ra in control and IL-6 treated co-culture media, an unpaired two-tailed t-test was employed. When comparing the mean between two distinct conditions, such as the concentrations of cytokines in control and IL-6 treated monoculture media from NPCs and MGLs, a two-way ANOVA was employed. In the cases where significant differences were observed between groups in these models, post-hoc testing was conducted using the Benjamini-Hochberg (BH) method with a false discovery rate (FDR) of 5% to identify the individual groups with significant differences. Adjusted p-values (q-values) less than 0.05 were considered statistically significant, and relevant significant q-values are quoted. The BH correction method with a 5% FDR threshold was also employed when deciphering the differentially expressed genes from each transcriptome signature, and during the RNAseq downstream over representation analysis.

Results

Neural progenitor cells respond to IL-6 by trans-signalling in the presence of sIL-6Ra in a dose-dependent manner

To investigate the possibility that NPCs can respond to IL-6 via trans-signalling using sIL-6Ra, we introduced recombinant human sIL-6Ra (rIL-6Ra) to forebrain NPC monocultures derived from three male donors without a psychiatric diagnosis (one clone each) at day (D) 18 of differentiation. We measured by the phosphorylation of STAT3 protein (pSTAT3) levels via immunoblotting to determine if exogenous rIL-6Ra

could facilitate a response to IL-6 (Figure 1A). Following the combined treatment of 100ng/ml rIL-6Ra and 100ng/ml IL-6, we observed a significant increase in STAT3 phosphorylation in D18 NPCs after 15 minutes (one-way ANOVA $F(3, 8) = 1773$, $p < 0.0001$), which, while reduced, remained detectable at 3 hours (one-way ANOVA $F(3, 8) = 4.920$, $p = 0.0318$) (Figure 1B). Furthermore, a dose-dependent relationship was evident when varying rIL-6Ra concentrations (Figure 1C). Lower doses corresponded to reduced pSTAT3/tSTAT3 ratios after 15 minutes of IL-6 exposure (two-way ANOVA: Interaction $F(4, 20) = 31.94$, $p < 0.0001$; [rIL-6Ra] Factor $F(4, 20) = 36.55$, $p < 0.0001$; Treatment Factor $F(1, 20) = 436.0$, $p < 0.001$) (Figure 1D, statistics in Supplementary Table 3). Notably, at the lowest dose (1ng/ml rIL-6Ra), there was no statistical difference between pSTAT3/tSTAT3 levels in vehicle and IL-6 treated NPCs (5% FDR = 0.371). These findings are consistent with those of Sarieva and colleagues (2023) and suggest that D18 NPCs can respond to IL-6 stimulation in the presence of exogenous sIL-6Ra via trans-signalling as well as hyper-IL6. We extend this data to show the dose-dependency of STAT3 phosphorylation on the concentration of rIL-6Ra. These data suggest that NPCs have the potential to respond to IL-6 by trans-signalling, via soluble IL-6R released from microglia in co-culture.

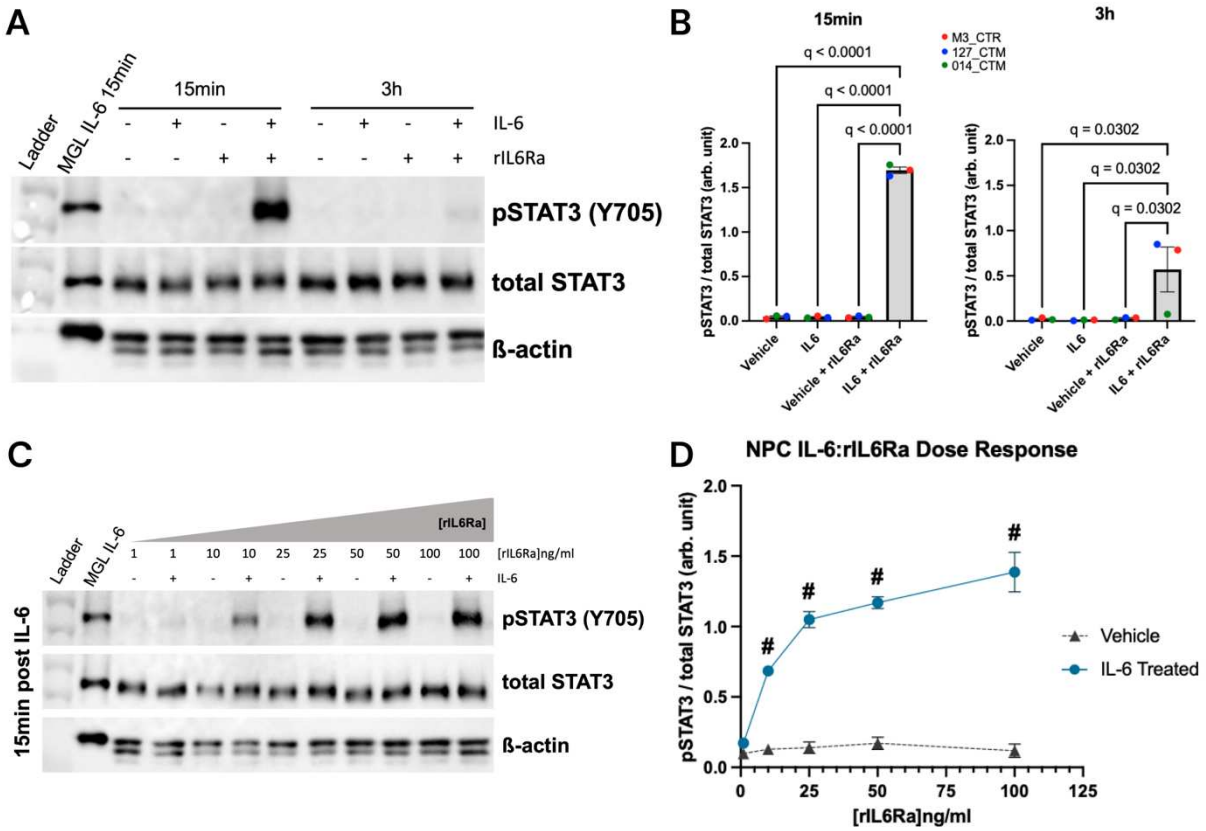

Figure 1 – Demonstrating Trans-Signalling Capability of Cortical Neural Progenitor Cells with IL-6 in Monoculture. (A) Immunoblot depicting pSTAT3 (88kDa), tSTAT3 and β-Actin protein levels in D18 NPC monocultures. Samples, treated with vehicle or 100ng/ml IL-6 coupled with or without 100ng/ml of sIL-6Ra, were collected at 15 minutes and 3 hours for comparison. (B) Quantitative assessment of pSTAT3/tSTAT3 protein ratios from blot (A) at 15 minutes and 3 hours post-stimulation. Measurements are in arbitrary units, presented as mean ± standard deviation (SD). Statistical significance determined by one-way ANOVA with 5% FDR (Benjamini–Hochberg method) is indicated. Data derived from N=3 neurotypical male hiPSC cell lines, each with one technical replicate. Data points are colour-coded per donor line: red for M3_CTR, blue for 127_CTM, and green for 014_CTM. (C) Immunoblotting results showing 88kDa pSTAT3/tSTAT3 and β-Actin in response to a gradient of rIL-6Ra concentrations (1, 10, 25, 50, and 100 ng/ml) combined with 100ng/ml IL-6. Samples collected after 15 minutes of stimulation in D18 NPC monocultures. (D) Line graph quantification of pSTAT3/tSTAT3 protein ratios from blot (C) at 15 minutes and 3 hours, presented in arbitrary units. Data points are mean ± SD, with colour-coding indicating treatment conditions as per the key. Two-way ANOVA results, with adjustments for multiple comparisons and a q-value < 0.0001 after 5% FDR correction, are marked with '#' for IL-6 treatment vs. vehicle comparisons. Data based on N=3 neurotypical male hiPSC cell lines, each with one technical replicate.

The concentration of sIL6Ra released from hiPSC-derived MGLs may not be sufficient to induce trans-signalling in NPCs

If NPCs in co-culture are to respond via trans-signalling to IL-6, then the presence of sIL-6Ra secreted by microglia is evidently required. To confirm this, we measured sIL-6Ra concentrations in an MGL-NPC co-culture media using ELISA (Figure 2A). The results confirm the presence of the soluble receptor, but there were no significant changes in sIL-6Ra concentration after 24h of IL-6 exposure (unpaired two-tailed t-test $t(6) = 0.180$, $R2 = 0.005$, $p = 0.863$). The average concentration of sIL6-Ra in the media was 0.29 ± 0.03 ng/ml, (range: 0.27 to 0.31 ng/ml). This concentration is below the apparent threshold required for NPCs to respond to exogenously added recombinant sIL-6Ra, as indicated in Figure 1C ([sIL-6Ra] < 1 ng/ml in culture media). Moreover, it is lower than the average sIL-6Ra concentration found in human cerebrospinal fluid (CSF), which is typically around 1.3 ± 0.6 ng/ml in inflammatory patients (meningitis symptoms with pleocytosis) and 0.9 ± 0.5 ng/ml in non-inflammatory patients (meningitis symptoms without pleocytosis) (Azuma *et al.*, 2000). Of note, the Asp358Ala A>C *IL6R* variant is known to increase sIL-6Ra secretion whilst conversely reduce a cell's overall responsiveness to IL-6 (Ferreira et al., 2013; Khandaker et al., 2014). We therefore next characterized this SNP in our donor lines to mitigate potential confounding effects on our ELISA results. Genotyping revealed that all donor lines used in this study possessed the C/C allele (Supplementary Table 5). However, despite this genetic inclination towards higher sIL-6Ra levels, our findings indicate that although the sIL-6Ra receptor is present, the co-culture system concentration might still be insufficient for effective NPC trans-signalling during the 24-hour exposure period in the experimental set-up chosen.

Irrespective of IL-6 trans-signalling in the NPCs, we hypothesized that NPCs might additionally react to other cytokines produced by MGLs in response to IL-6 stimulation. To investigate this, we used a qualitative cytokine profiler to characterize the cytokine and chemokine milieu in the co-culture media following 24 hours of exposure to IL-6 or a vehicle control (Figure 2C). This analysis included a panel of 105 cytokines and chemokines (Supplementary Figure 5). We observed that osteopontin, IL-8, ENA-78, and MMP-9 were the most abundant molecules in the co-culture media across both treatment groups (Figure 5C). Relative to the vehicle control, IL-6 exposure led to increased signals in 78 molecules and a decrease in 26. The five most upregulated molecules were MIP-1α/MIP-1β (Fold Change (FC) = 4.153), RANTES (FC = 2.118), GROα (FC = 2.105), TNF-α (FC = 1.689), and PF4 (FC = 1.593). Conversely, the most significantly downregulated molecules included anti-inflammatory ligands Lipocalin-2 (FC = 0.69), PDGF-AA (FC = 0.69), LIF (FC = 0.82), and Fas Ligand (FC = 0.88). The overall qualitative profile of these cytokines and chemokines suggests a shift towards a pro-inflammatory environment, associated with the recruitment and activation of additional immune cells. This is further highlighted by the decreased presence of molecules typically linked to dampening inflammation, neuroprotection, and regeneration (Hinks and Franklin, 1999; Diemel, Jackson and Cuzner, 2003; Lee *et al.*, 2007; Zhao *et al.*, 2018; Lin *et al.*, 2020). This pattern of cytokine and chemokine secretion points to a transition from a restorative environment towards a more pronounced immune defence response in the co-culture system, extending similar results from the MGL secretome response to IL-6 in monoculture (Couch *et al.*, 2023).

To corroborate the findings from the proteome profiler assay, we quantitatively measured four cytokines using a multiplex cytokine assay by Meso Scale Diagnostics

(Figure 2D). MIP-1α and TNF-α were selected for their upregulation in response to IL-6, while IL-8 served as a negative control due to its consistent secretion levels in both vehicle and IL-6 treated media. Additionally, VEGF was included due to its role in angiogenesis and neurodevelopment, given its observed increased expression in chronic medicated SZ patients (Chukaew *et al.*, 2022) and in foetal mouse brains from an MIA rodent model (Poly I:C on gestational day 16) (Arrode-Brusés and Brusés, 2012). Consistent with our expectations, IL-8 levels remained stable with IL-6 treatment (unpaired two-tailed t-test: $t(6) = 1.603$, $R2 = 0.30$, $p = 0.160$). MIP-1α showed an increase following IL-6 treatment, though not reaching statistical significance (unpaired two-tailed t-test: Fold Change (FC) = 2.48, $t(6) = 2.220$, $R2 = 0.451$, $p = 0.0682$). TNF-α levels, on the other hand, exhibited a significant rise upon IL-6 exposure (unpaired two-tailed t-test: FC = 13.75, $t(6) = 2.628$, $R2 = 0.535$, $p = 0.039$). In contrast, VEGF-A levels did not significantly change with IL-6 treatment (unpaired two-tailed t-test: FC = 1.155, $t(6) = 0.202$, $R2 = 0.007$, $p = 0.847$). Overall, the expression patterns of these cytokines quantitatively measured by the multiplex cytokine assay aligned with the qualitative trends observed in the proteome profiler assay, reinforcing our understanding of the cytokine response to IL-6 in our experimental setup.

Finally, to elucidate the source of cytokine secretion in our co-culture system, we examined the same cytokine candidates in 24-hour IL-6 treated D14 MGL and D18 NPC monocultures derived from N = 3 neurotypical male cultures (Figure 2D, with two-way ANOVA statistics provided in Supplementary Table 7). Our analysis indicated that MGLs were predominantly responsible for secreting IL-8, MIP-1α, and TNF-α, whereas VEGF secretion was mainly attributed to NPCs. Notably, TNF-α was the only

cytokine to demonstrate a statistically significant increase in response to IL-6 treatment in MGLs (MGL Vehicle vs MGL IL-6, q = 0.015), but not in NPCs. In fact, hiPSC-derived NPCs from the same protocol do express the necessary receptors to respond to TNF-α (*TNFRSF1A/B*) (Couch *et al.*, 2023), so we could reasonably expect a response by the cell after TNF-α secretion from MGLs in co-culture. Together, the data provide insights into the cytokine milieu downstream of IL-6 signalling in an MGL-NPC co-culture system, and the cytokines to which NPCs may respond within the co-culture environment in addition to direct IL-6 trans-signalling.

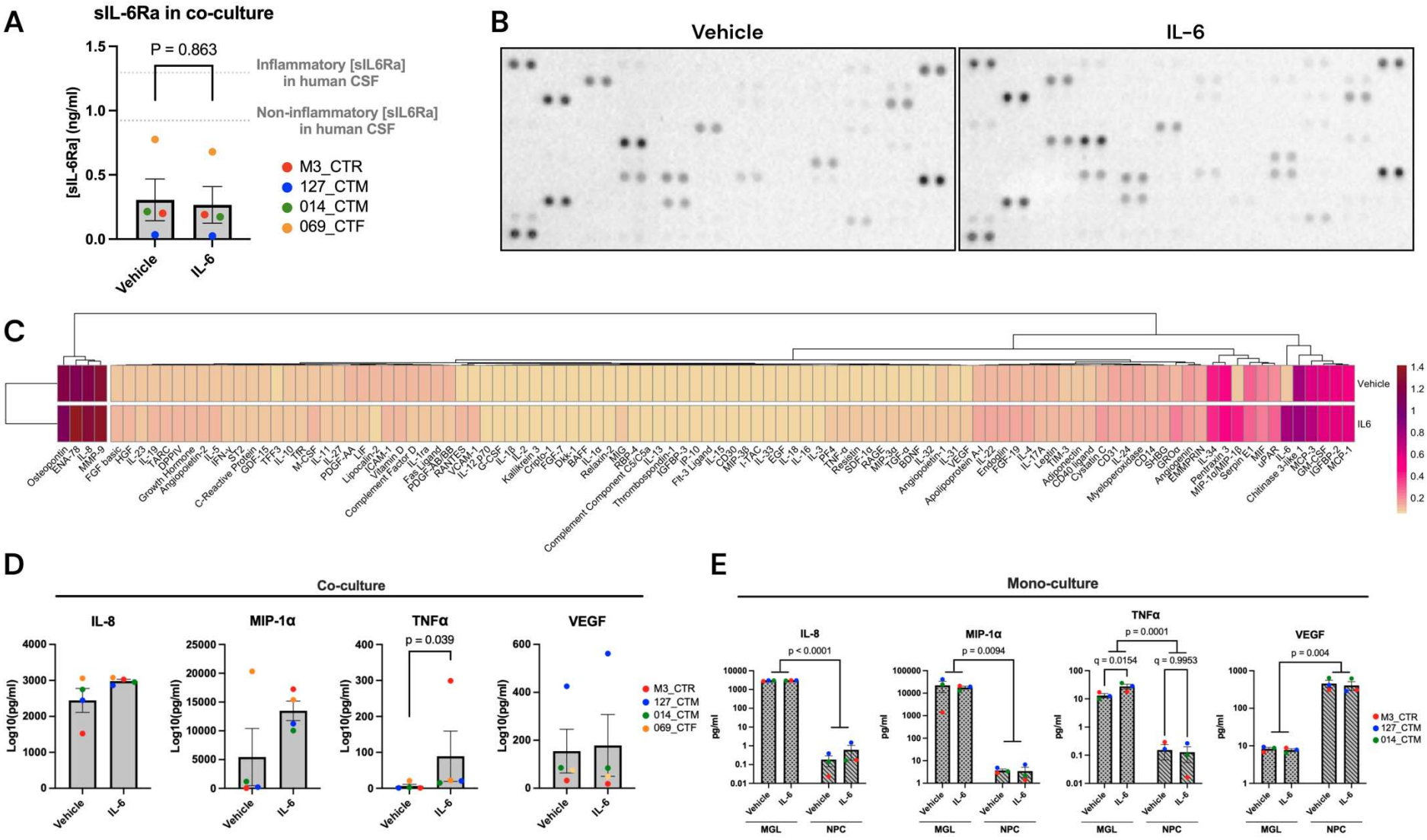
A
sIL-6Ra in co-culture
P = 0.863
Inflammatory [sIL6Ra] in human CSF
Non-inflammatory [sIL6Ra] in human CSF
[sIL-6Ra] (ng/ml)
1.5
1.0
0.5
0.0
Vehicle
IL-6
M3_CTR
127_CTM
014_CTM
069_CTF
B
Vehicle
IL-6
C
Vehicle
IL6
1.4
1.2
1
0.8
0.6
0.4
0.2
Osteopontin
ENA-78
IL-8
MMP-9
FGF basic
HGF
IL-23
IL-19
TARC
DPPIV
Growth Hormone
Angiopoietin-2
IL-5
IFN-γ
ST2
C-Reactive Protein
GDF-15
TFF3
IL-10
TfR
M-CSF
IL-11
IL-27
PDGF-AA
LIF
Lipocalin-2
ICAM-1
Vitamin D
Complement Factor D
IL-1ra
Fas Ligand
RAGE
PDGF-AB/BB
RANTES
VCAM-1
IL-12 p70
G-CSF
IL-1β
IL-2
Kallikrein 3
Cripto-1
FGF-7
Dkk-1
BAFF
IL-1α
Relaxin-2
MIG
RBP-4
Complement Component C5/C5a
IL-13
Thrombospondin-1
IGFBP-3
IP-10
Flt-3 Ligand
IL-15
CD30
MIP-3β
I-TAC
IL-33
EGF
IL-18
IL-16
IL-3
PF4
TNF-α
Resistin
SDF-1α
RAGE
MIP-3α
TGF-α
BDNF
IL-32
Angiopoietin-1
IL-31
VEGF
Apolipoprotein A-I
IL-22
Endoglin
FGF-19
IL-4
IL-17A
Leptin
TIM-3
Adiponectin
CD40 ligand
Cystatin C
CD31
IL-24
Myeloperoxidase
CD14
SHBG
GROα
Angiopoietin
EMMPRIN
IL-34
Pentraxin 3
MIP-1α/MIP-1β
Serpin E1
MIF
uPAR
IL-6
like-1
MCP-3
GM-CSF
IGFBP-2
MCP-1
Chitinase 3-like 1
D
Co-culture
IL-8
MIP-1α
TNFα
p = 0.039
VEGF
Log10(pg/ml)
Vehicle
IL-6
M3_CTR
127_CTM
014_CTM
069_CTF
E
Mono-culture
IL-8
p < 0.0001
MIP-1α
p = 0.0094
TNFα
p = 0.0001
q = 0.0154
q = 0.9953
VEGF
p = 0.004
pg/ml
MGL
NPC
M3_CTR
127_CTM
014_CTM

Figure 2 - Investigating Indirect Effects of IL-6 Through the MGL Cytokine Secretion Response. (A) The sIL-6Ra concentration in co-culture media (ng/ml) varied by donor without significant IL-6 treatment effects. Data points are color-coded by donor and presented as mean ± SD. Reference lines indicate typical human CSF sIL6Ra levels in control (non-inflammatory) and meningitis (inflammatory) cases, based on Azuma et al. (2000). (B) The cytokine profiles in vehicle and IL-6 treated NPC-MGL co-cultures as measured by dot blot images comparing cytokine secretion, using the Proteome Profiler Human XL Cytokine Array Kit (R&D Systems) measuring 104 cytokines (N = 4 donors pooled per condition). Cytokine and chemokine labels provided in supplementary material. (C) Heatmap of raw cytokine signals from the Proteome Profiler Array. Plotted are averaged raw signal values from 2 technical replicates per cytokine, with IL-6 added during treatment. (D) Concentrations of MIP-1a, TNF-α, IL-8, and VEGF-A measured in co-culture media after 24h with vehicle or 100ng/ml IL-6 treatment (N = 4, grey bars), as measured by the MSD multiplex cytokine assay. Results are plotted as Log10(pg/ml), with unpaired two-tailed t-test p-values annotated for significant comparisons (non-significant values unlabelled). Bar graphs show mean ± SD, coloured by donor line. (E) Concentrations of MIP-1a, TNF-α, IL-8, and VEGF-A in monoculture media from control donors (N = 3 males) D14 MGLs and D18 NPCs, treated for 24h with vehicle or 100ng/ml IL-6, as measured by the MSD multiplex cytokine assay. Data plotted as pg/ml on a log scale. 5% FDR corrections post two-way ANOVA indicated. Bar graphs represent mean ± SD, color-coded by donor line.

The impact of acute IL-6 on hiPSC-derived MGL transcriptome after 24h

In addition to the secretome, bulk RNAseq analysis was conducted to characterize and confirm the overall transcriptional response of hiPSC-derived microglia-like cells (MGLs) in co-culture with neural progenitor cells (NPCs) to IL-6. Principal component analysis (PCA) of each sample highlighted the most significant variance in the MGL transcriptome: donor genetic background (PC1 = 58% variance explained) and IL-6 treatment (PC2 = 19.64% variance explained) (Figure 3A). Notably, the only female donor (069_CTF) exhibited distinct separation on the PC1 axis from male donors, but due to inclusion of a single female hiPSC line, further sex-based analysis was not pursued. Subsequent analysis revealed 72 differentially expressed genes (DEGs) post-IL-6 exposure (out of 16820 genes measured) after FDR correction at 5%. As anticipated, similarly to our prior study with IL-6 stimulated MGL mono-cultures (Couch *et al.*, 2023), IL-6 receptor signal transduction genes like *JAK3* and *STAT3* were significantly upregulated (Figure 3B). The most upregulated gene was *EBI3*, known

for mediating IL-6 trans-signalling, albeit less efficiently than sIL-6Ra (Chehboun *et al.*, 2017). These results confirm successful IL-6 stimulation in control MGLs in co-culture.

We also validated the MGL differentiation from hiPSCs and assessed if IL-6 stimulation influenced their inherent cell type identity. The DESeq2 normalized counts of human microglia and monocyte marker genes were compared between vehicle-treated and IL-6 treated samples (Figure 3C). This comparison was based on a gene list from Haenseler et al. (2017), including genes highly expressed in human microglia (Melief *et al.*, 2012) and *TMEM119*, a microglia-specific gene (Bennett *et al.*, 2016). Our findings align with the expression profile of microglial marker genes as per the original MGL differentiation protocol, and no significant clustering was observed based on IL-6 treatment, suggesting that IL-6 exposure did not alter MGL cell-specificity at the gene expression level, consistent with previous data (Couch *et al.*, 2023).

To explore the molecular pathways influenced by IL-6 receptor signalling in MGLs in co-culture with NPCs, we conducted a Webgestalt over-representation analysis (ORA) on the up- and down-regulated gene sets (Liao *et al.*, 2019) (Figure 3D). The down-regulated gene set showed no significant associations with ORA pathways post-FDR correction ($q > 0.05$). In contrast, 24 pathways were significantly linked with upregulated genes, including “STAT cascade”, “Interleukin-6 production”, and “acute inflammatory response” (Figure 3D). The pathway “positive regulation of cell motility” was also notably associated, supporting previous findings that IL-6 stimulation enhances microglial motility (Ozaki *et al.*, 2020; Couch *et al.*, 2023). These data suggest that the observed terms related to the IL-6 pathway, along with others

pertaining to cellular recruitment and cell-to-cell adhesion (such as "leukocyte migration", "T-cell activation", and "regulation of cell-cell adhesion"), point towards an acute, pro-inflammatory functional shift by the microglia to an acute 24h stimulation with IL-6 in co-culture with NPCs.

To understand if the IL-6-induced transcriptional changes in MGLs after 24 hours mirror those observed in neurodevelopmental disorders, we performed gene set enrichment analysis (GSEA) (Figure 3E). The analysis overlapped each signature with gene sets from post-mortem brain tissue of individuals with schizophrenia (SZ), autism spectrum conditions (ASC), and bipolar disorder (BD). Notably, the MGL transcriptome post-IL-6 exposure showed significant enrichment for the up-regulated gene set from SZ patients. Webgestalt ORA identified several enriched pathways, including “lymphocyte activation”, “adaptive immune response”, and “T cell activation” (Figure 3F). Collectively, these findings imply that the IL-6 response of MGLs in co-culture mirrors that observed in monocultures (Couch *et al.*, 2023), and that the molecular processes identified in SZ post-mortem brain tissue are detectable in our developmental *in vitro* model.

Finally, we aimed to delineate the differences between the MGL transcriptomic response to IL-6 in co-culture versus mono-culture conditions (Couch et al., 2023). To achieve this, we utilised the MGEnrichment tool output to qualitatively compare specifically human modules that were enriched by up-regulated genes in both the mono-culture and co-culture MGLs following IL-6 stimulation (Figure 3G). Firstly, the enrichment scores derived from our MGEnrichment analysis demonstrated a robust

activation of the 'SCZ & ASD & BD Gene Modules' within the co-culture environment as well as the mono-culture environment, indicating a highly potentiated upregulation of genes associated with NDDs (co-culture FE = 12.36, q = $2.14x10^{-11}$). This pronounced response contrasted with the more modest enrichment scores obtained from the mono-culture microglia (mono-culture FE = 5.07, q = $1.8x10^{-13}$). Furthermore, gene modules associated with core microglial signatures and anti-inflammatory responses also showed a lesser enrichment than that in mono-culture. These data suggest that the presence of NPCs in the co-culture not only enhances the MGL response to IL-6 but also appears to modulate the regulation of genes across a broad spectrum of pathways, particularly those pertinent to NDDs. This enhancement suggests a nuanced interplay where NPCs contribute to a microenvironment that is more conducive to the expression of genes within NDD-related gene sets. Consequently, this underscores the critical importance of co-culturing multiple cell types *in vitro* for more accurate modelling of NDDs using hiPSCs, consistent with previous data (Haenseler *et al.*, 2017).

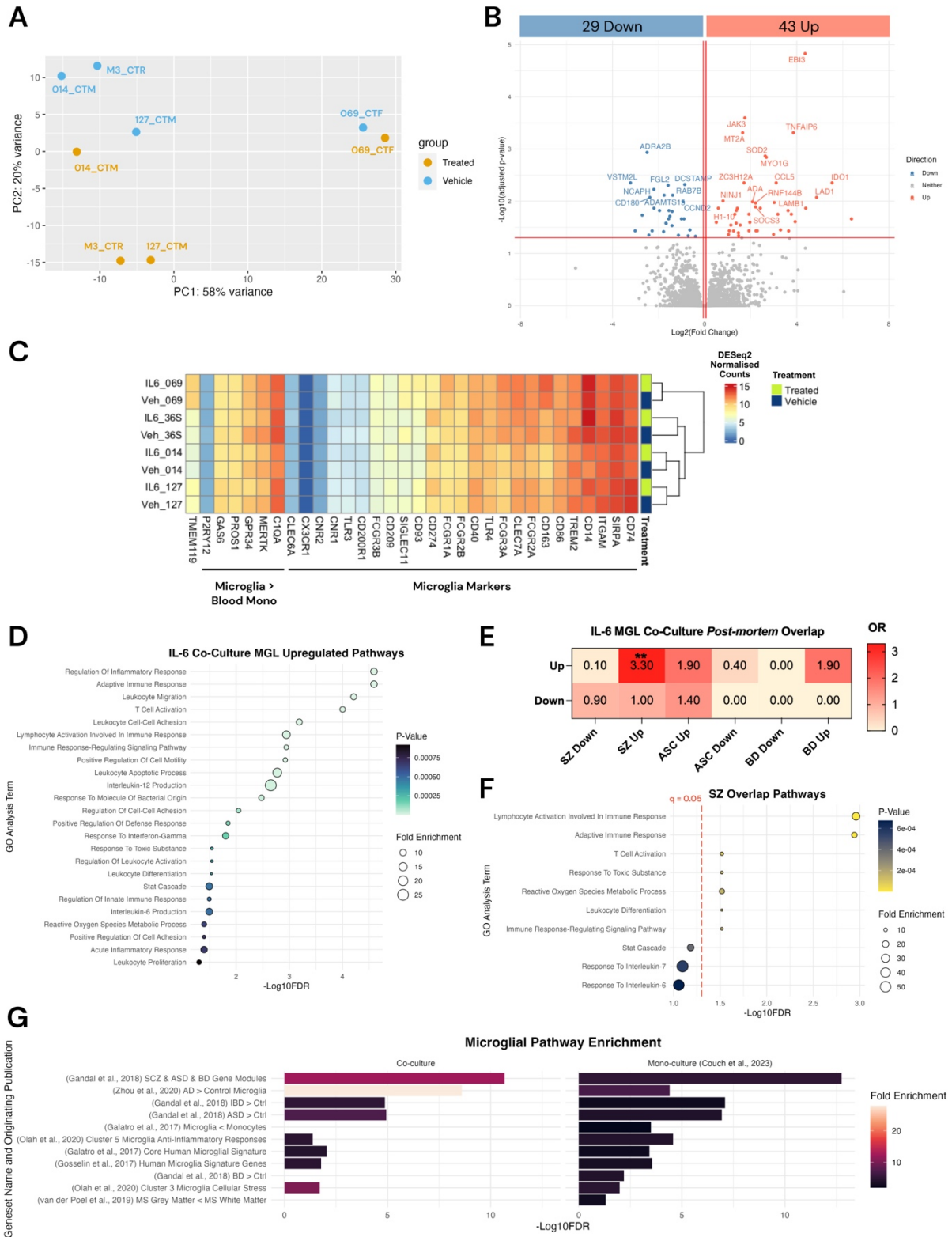

Figure 3 - IL-6 Induces Changes in the MGL Transcriptome in Co-Culture with NPCs. (A) PCA of DESeq2 normalized counts (median of ratios), colour-coded for vehicle (blue) and IL-6 treatment (orange) and identified by donor line. Clustering reveals treatment and donor genotype influences on the MGL transcriptome. (B) Volcano plot highlighting 72 differentially expressed genes in MGLs post 24h IL-6 stimulation in co-culture with NPCs. Genes with log2FoldChange > 0.06 and adjusted p-value < 0.05 are marked in red; those with log2FoldChange < -0.06

and adjusted p-value < 0.05 in blue. Top 25 DEGs are labelled. (C) Heatmap of DESeq2 normalized counts (median of ratios) for vehicle-treated MGLs, showing consensus microglial-specific markers, including genes highly expressed in human microglia and those differentially expressed compared to blood monocytes, plus TMEM119. Right-hand side hierarchical clustering indicates no significant treatment-based changes. (D) Webgestalt gene ontology analysis of upregulated genes post-IL-6 treatment in MGLs, with 5% FDR correction. ORA terms sorted by –log10FDR, colour-coded by p-value, and scaled by fold enrichment. (E) Fisher's exact test comparing gene sets from ASC, SZ, and BD post-mortem human tissues (Gandal et al., 2018) with RNAseq-identified up- and down-regulated gene sets. Heatmap of odds ratios (OR) presented, with significance marked as: . q < 0.1, * q < 0.05, ** q < 0.01, *** q < 0.001, **** q < 0.0001; non-significant values are unlabelled. (F) Webgestalt gene ontology analysis of the 17 genes common between MGL up-regulated IL-6 and upregulated SZ post-mortem tissue gene sets (Gandal et al., 2018). Analysis is FDR-corrected at 5%, with ORA terms sorted by –log10FDR, colour-coded by p-value, and sized by fold enrichment. Red dotted line signifies q = 0.05, and values to the left of this line do not pass BH FDR correction. (G) MGEnrichment analysis of genes up-regulated in IL-6 stimulated MGLs, in both co-culture and mono-culture settings (Couch et al., 2023), adjusted with a 5% FDR. Enriched gene sets arranged by –log10FDR and colour-coded by fold enrichment.

The proximal impact of IL-6 on hiPSC-derived NPC transcriptome in co-culture with MGLs

With the knowledge that hiPSC-derived MGLs responded to IL-6 in co-culture with NPCs, we aimed to investigate if NPCs respond to IL-6 via trans-signalling either directly from sIL6Ra secreted by MGLs, or indirectly via other cytokines and chemokines such as TNF-α secreted by MGLs in response to IL-6. Bulk RNAseq was performed on hiPSC-derived NPCs after 24 hours in co-culture with MGLs treated with either IL-6 or vehicle. We first assessed the impact of co-culturing NPCs with MGLs and IL-6 treatment on cell type heterogeneity using the NPC RNAseq dataset (Figure 4A). DESeq2 normalized counts were analysed for markers indicative of neural progenitor, pan-neuronal, dorsal forebrain, ventral forebrain, midbrain, hindbrain, upper layer and deep layer cells (Nehme *et al.*, 2018) (Figure 4A). The analysis revealed predominant expression of neural progenitor cell-related genes, consistent with the expected outcome at this differentiation stage. This finding suggests that co-culturing with hiPSC-derived MGLs using trans-well inserts did not alter the anticipated

NPC cell type profile, given there was no hierarchical clustering by cell-markers. Clustering was in-fact influenced by donor genotype rather than IL-6 treatment, indicating that the IL-6 exposure did not significantly affect the cell type composition of NPCs at this culture stage.

Contrary to our hypothesis however, NPCs exhibited a minimal transcriptional difference when cultured in trans-well co-culture with microglia and stimulated with IL-6. PCA analysis revealed that the most significant variation in the NPC transcriptome was attributable to donor genotype rather than IL-6 treatment (Figure 4B). Out of the 17225 genes measured, only 2 DEGs passed the 5% FDR threshold for increased expression in NPCs in co-cultures treated with IL-6 versus vehicle (Figure 4C): TNF-Alpha-Induced Protein 3 (*TNFAIP3*: q = 0.0282, Log2FC = 1.545) and Poly(A) Binding Protein Cytoplasmic 1 (*PABPC1*: q = 0.0282, Log2FC = 0.1874). *TNFAIP3* is known for its role in cytokine-mediated immune responses and was previously reported to be upregulated in neural stem cells infected with ZIKA virus (McGrath *et al.*, 2017). *PABPC1* is involved in ribosomal recruitment and protein synthesis (Kawahara *et al.*, 2008). The absence of statistically significant changes in JAK/STAT pathway genes (*STAT3* Log2FC = 0.0997, p = 0.543, q = 0.9998; *JAK3* Log2FC = 0.584, p = 0.0396, q = 0.9998, Supplementary Figure 2) suggests that the IL-6-receptor signal transduction pathway was not activated in NPCs at the timepoint of analysis, in contrast to MGLs (Supplementary Figure 2). On the other hand, the data suggests that the NPCs might have the potential to react to the TNF-α secreted by MGLs cells, as indicated by the observed upregulation of *TNFAIP3*. In summary, under the tested

conditions, NPCs derived from neurotypical control donors exhibit a negligible or limited transcriptional response to 24-hour IL-6 exposure in co-culture with MGLs.

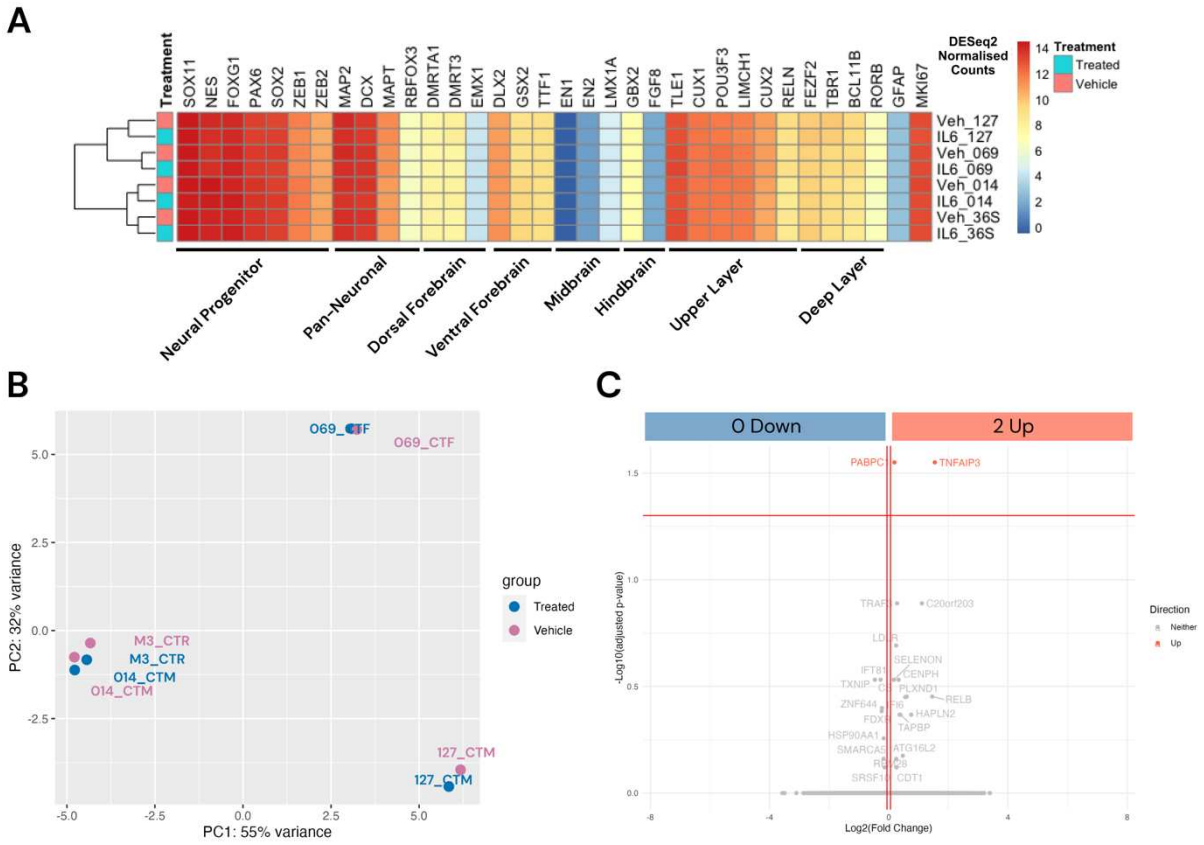

Figure 4 - Assessing the Proximal NPC Transcriptome Response to IL-6 in Co-Culture with MGLs. (A) Heatmap of DESeq2 normalized counts (median of ratios) from vehicle-treated NPCs, displaying cell-specific marker gene expression across both genotypes. (B) PCA plot of DESeq2 normalized data (median of ratios), distinguishing vehicle (pink) and IL-6 treated (blue) samples, with donor line annotations. (C) Volcano plot showcasing NPCs' differentially expressed genes following IL-6 exposure in co-culture with MGLs. Genes with log2FoldChange > 0.06 and adjusted p-value < 0.05 are marked in red; those with log2FoldChange < -0.06 and adjusted p-value < 0.05 in blue. Genes without a significant FDR corrected p-value are coloured grey. The top 25 expressed genes are labelled.

The long-term impact of acute NPC-stage IL-6 exposure in terminally differentiated cortical neurons

To evaluate whether IL-6 exposure to MGL-NPC co-cultures, either directly via trans-signalling or indirectly via the response secretome by MGLs, influenced the

differentiation trajectories of forebrain NPCs at D18 in co-culture with MGLs, we analysed the relative proportions of cell types using cell-specific markers. Cell counts immunopositive for TUJ1, GFAP and Pax6 were quantified as a percentage of total cells in terminally differentiated cortical neuron cultures at day 50 of differentiation (Figure 5B). The results showed that across both treatment groups, 96.66% of all cells were TUJ1+, 17.27% were GFAP+, and 6.38% were Pax6+, suggesting a predominance of neurons in the differentiated cultures (Figure 6.3B). The majority of cells in both treatment groups were TUJ1+/GFAP-/Pax6- (73.43 ± 5.37%), indicating a significant proportion of neurons, followed by cells likely representing foetal astrocytes or radial glia (TUJ1+/GFAP+/Pax6-; 16.72 ± 3.04%) (Dráberová *et al.*, 2008). A limited population only expressed Pax6 (TUJ1-/GFAP-/Pax6+ = 2.82 ± 1.00 %), and with minimal co-expression with TUJ1 (TUJ1+/GFAP-/Pax6+ = 3.49 ± 1.05 %) (Figure 5B). Notably, there were no significant differences in the proportions of cell types between NPCs exposed to IL-6 and those that were not (two-way ANOVA: treatment $F(1,42) = 2.25x10^{-7}$, $p = 0.999$; cell-type $F(6,42) = 88.04$, $p < 0.0001$; interaction $F(1=6,42) = 0.38$; $p = 0.89$). In summary, these findings indicate that NPCs in co-culture with MGLs differentiated into a range of cell types, predominantly post-mitotic cortical neurons, and that IL-6 exposure did not significantly alter their differentiation towards various cell fates.

The architecture, number, and source of synaptic connections on neurons critically influence neuronal activity (Kuljis *et al.*, 2019). Furthermore, disruptions in these synaptic properties could be central to the pathogenesis of NDDs (Bayés *et al.*, 2011; Südhof, 2017; Mirabella *et al.*, 2021). We therefore explored whether changes during the NPC stage, either directly by trans-IL-6 signalling or indirectly via cytokines

released from IL-6 stimulated MGLs, could induce alterations in synapses. To investigate this, we quantified the density and abundance (by signal intensity) of both inhibitory and excitatory synaptic puncta along MAP2+ neurites, grown until D50 of differentiation. The choice of synaptic markers was informed by their relevance to synaptic transmission and association with neurodevelopmental disorders such as SZ and ASC. Specifically, we focused on PSD95 (Figure 5C), GluN1 (Figure 5D), and vGlut1 (Figure 5C) due to their roles in glutamatergic neurotransmission. Dysregulation in this system has been implicated in the onset of SZ and ASC (Oni-Orisan *et al.*, 2008; Bitanihirwe *et al.*, 2009; Moghaddam and Javitt, 2012; Holloway *et al.*, 2013; De Bartolomeis *et al.*, 2014; Grunwald *et al.*, 2019; Mirabella *et al.*, 2021). Additionally, SV2A (Figure 5D) was included due to its reported decrease in individuals with an SZ diagnosis (Onwordi *et al.*, 2020, 2023). We also assessed GAD67 (Figure 5E), known for its consistently decreased expression in the brains of individuals with psychiatric disorders such as SZ, bipolar disorder (BD), and major depressive disorder (MDD) (Miyata et al., 2021; Karolewicz et al., 2010; Hashimoto et al., 2008; Guidotti et al., 2000). Lastly, Gephyrin was examined due to its association with hemizygous microdeletions in the G-domain (Figure 5E), which have been observed in unrelated individuals affected by ASC and SZ (Lionel *et al.*, 2013).

However, under the tested conditions, early IL-6 exposure at the NPC stage did not significantly affect the densities, nor the abundance of either pre- or post-synaptic protein expression, as measured by the non-parametric Wilcoxon's test (Figure 5F). Furthermore, we investigated the co-localization of pre- and post-synaptic proteins: PSD95 with vGlut1, GluN1 with SV2A, and Gephyrin with GAD67 (Supplementary Figure 3). The extent of puncta co-localization, interpreted as pre- and post-synaptic

connectivity, was quantified and compared between vehicle-treated neurons and those exposed to IL-6. Our results indicate that puncta co-localization was not influenced by early acute IL-6 exposure, as evidenced by the absence of significant differences between the treatment groups (Figure 5G, Supplementary Figure 4). However, there was clearly extensive donor variance in these measures following exposure to IL-6, likely due individual genotype differences. Hence, we cannot conclusively dismiss the possibility of an effect of IL-6.

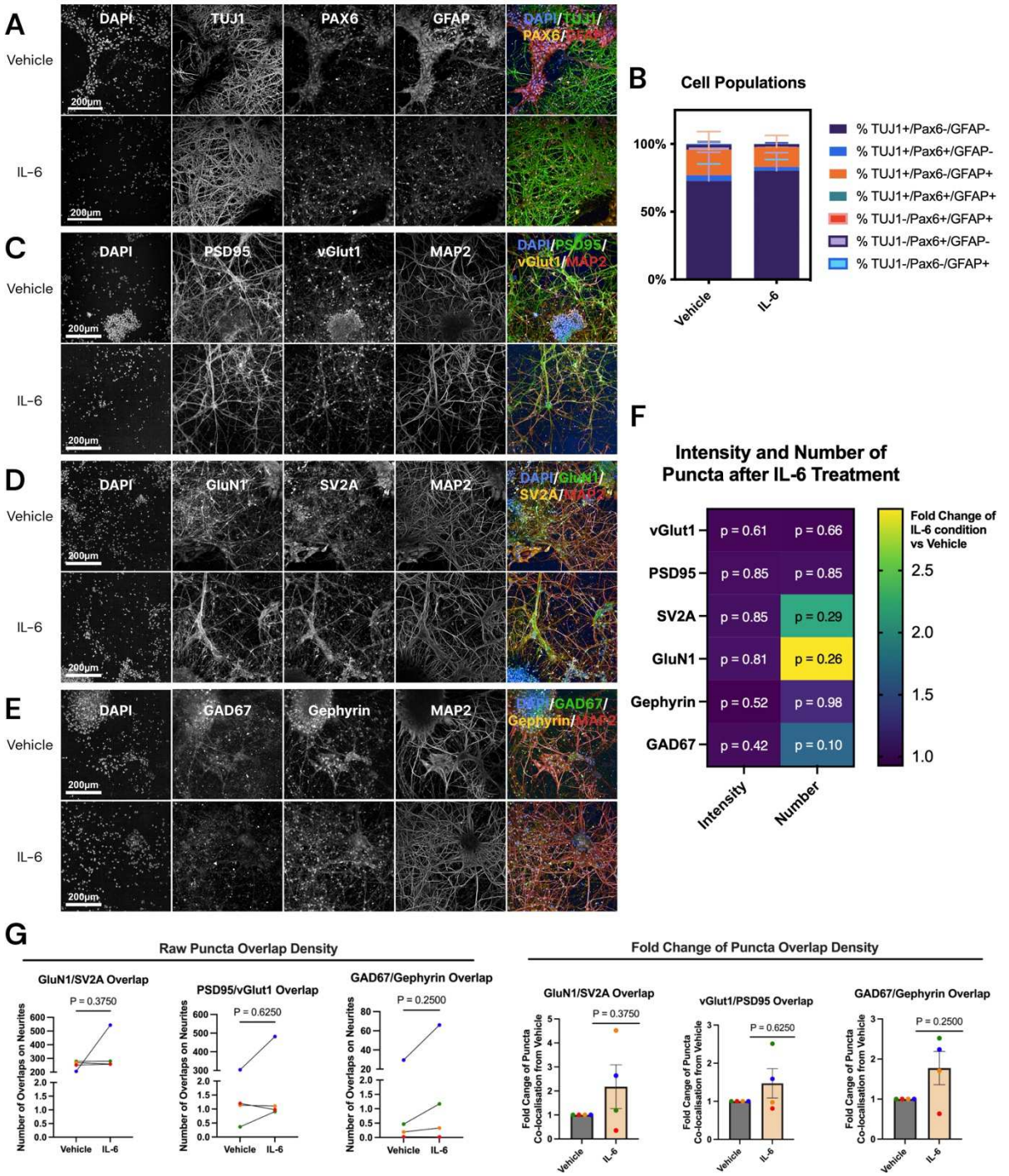

Figure 5 - The Long-Term Effect on Terminal Neuron Differentiation After IL-6 Stimulation of NPC in Co-Culture with MGLs. (A) Representative images of cortical neurons from donor 127_CTM_01, exposed to vehicle or IL-6 in co-culture with MGLs at their NPC stage. Cells were stained for DAPI (column 1), TUJ1 (column 2), PAX6 (column 3) and GFAP (column 4). Channels were overlayed in column 5. Scale bar represents 200µm. (B) Cell populations as a percentage of total number of cells counted within each donor (N = 4 donors averaged from N= 4 technical well culture repeats each), averaged across all images to one single data point per donor. (C-E) Representative images of cortical neurons from healthy control donor 127_CTM_01, exposed to vehicle or IL-6 in co-culture with MGLs at their NPC stage. Scale bar represents 200µm. (C) Cells were stained for DAPI (column 1), PSD95 (column 2), vGlut1 (column 3) and MAP2 (column 4). (D) Cells were stained for DAPI (column 1), GluN1

(column 2), SV2A (column 3) and MAP2 (column 4). (E) Cells were stained for DAPI (column 1), Gephyrin (column 2), GAD67 (column 3) and MAP2 (column 4). (F) Heatmap of fold change and p-values from one-sample Wilcoxon tests comparing vehicle (value = 1) and IL-6 treated cultures for signal intensity and number of puncta in MAP2+ neurites imaged in figures C-E. Raw metrics were averaged to give one data point per donor, and then IL-6 treated culture values were calculated as a fold change from each donor's vehicle prior to statistical analysis. (G) Raw density of co-localisation events of puncta pairs (GAD67 with Gephyrin, GluN1 with SV2A and vGlut1 with PSD95). Wilcoxon test p-values labelled on graph compare vehicle and IL-6 treated cultures. Technical replicates were averaged to give one data point per donor. Bar graph plotted as mean with standard deviation (SD) error bars, and points coloured by donor line: red (M3_CTR), blue (127_CTM), green (014_CTM) and orange (069_CTF). (H) Fold-change from vehicle of co-localisation events of puncta pairs (GAD67 with Gephyrin, GluN1 with SV2A and vGlut1 with PSD95). One-sample Wilcoxon test p-values labelled on graph compare vehicle and IL-6 treated cultures. Similarly, metrics were averaged to give one data point per donor and then IL-6 treated culture values were calculated as a fold change from each donor's vehicle. Bar graph plotted as mean with standard deviation (SD) error bars, and points coloured by donor line: red (M3_CTR), blue (127_CTM), green (014_CTM) and orange (069_CTF).

Discussion

Our study aimed to determine the role of prenatal IL-6 signalling and how it might contribute to the risk of psychiatric disorders with a putative neurodevelopmental origin, by particularly focusing on the interactions between neural progenitor cells and microglia-like cells derived from human-induced pluripotent stem cells. Our findings demonstrated that NPCs in monoculture can respond to IL-6 via trans-signalling in the presence of a recombinant soluble IL-6 receptor, but this response was dose-dependent on the soluble receptor and minimal at lower concentrations. This finding aligns with earlier observation that NPCs do not respond to IL-6 in monoculture in the absence of exogenous IL-6Ra or hyper-IL-6 (Couch *et al.*, 2023; Sarieva, Hildebrand, *et al.*, 2023). We further demonstrated that MGLs secrete soluble IL-6R and other cytokines in response to IL-6, including TNF-alpha, which has been previously identified as a key effector molecule in rodent models of maternal immune activation (Potter 2023). Contrary to our hypothesis, NPCs displayed only a marginal transcriptional response to IL-6 stimulation when in co-culture with MGLs, with only two genes showing differential expression passing the FDR threshold. This finding

particularly contrasts the substantial transcriptional changes observed in MGLs, indicating cell-type specific sensitivities to IL-6 signalling, as previously described in mono-culture (Couch *et al.*, 2023). Moreover, concerning the enduring effects of short-term IL-6 exposure during the NPC stage, our findings revealed no marked changes in the differentiation paths of forebrain NPCs into diverse cell types. This contrasts with earlier findings in hiPSC-derived neuronal cultures that cell-fate acquisition is affected by IL-6 (Sarieva, Kagermeier, *et al.*, 2023), but noting that Sarieva at colleagues (2023) stimulated their cultures with hyper-IL-6 for five days. Furthermore, IL-6 exposure did not significantly affect synaptic densities or intensities in post-mitotic neurons, which was also unexpected given previous research suggesting that early IL-6 exposure has the potential to alter synaptogenesis in the hippocampus of a rodent model, perhaps highlighting potential regional or species differences in the effects of IL-6 on synaptogenesis (Samuelsson *et al.*, 2006; Mirabella *et al.*, 2021).

Why do we observe a lack of substantial transcriptional and cellular effects in NPCs co-cultured with MGLs and stimulated with IL-6, despite the MGLs secreting the soluble IL-6R and other cytokines? First, the sIL-6Ra concentration secreted by MGLs was (0.29 ng/ml), and this is below the concentration necessary to trigger STAT3 phosphorylation in NPCs in response to IL-6 and recombinant IL-6Ra (Figure 1C). Furthermore, the concentration of sIL-6Ra in our co-culture system is lower than that reported in human (adult) CSF under both basal and inflammatory disease states, acknowledging that we lack data on sIL-6Ra levels during human development in either state. Hence, there simply may not have been enough sIL-6Ra secreted by the microglia to initiate trans-signalling in the NPCs. These data highlight the importance of considering the overall cytokine milieu in our *in vitro* model. The co-culture

secretome analysis suggested that TNF-α secreted by microglia following stimulation with IL-6 could act as a potential downstream risk mediator in NPCs. This is supported by the knowledge that NPCs possess receptors for TNF-α (*TNFRSS1A/B)* at the relevant differentiation timepoint (Couch *et al.*, 2023)*,* and can respond to this cytokine in vivo following maternal immune activation (Potter *et al.*, 2023). Apart from TNF-α, the cytokines showing the greatest change in profiler signals following IL-6 stimulation in co-culture were MIP-1α/MIP-1β, RANTES, GROα, and PF4. Yet, RNAseq data from the NPCs reveal that this cell type is not likely to be the target for these cytokines, given they exhibit relatively low expression levels of specific cytokine receptors such as CCR1 and CXCR3 (normalized DESeq2 counts: 1.02 ± 0.05 and 1.85 ± 0.4, respectively) and align with those from previous forebrain transcriptomic sets (Zhang *et al.*, 2016; Nowakowski *et al.*, 2017). These data highlight the significance of incorporating microglia in *in vitro* NDD models, but also cell types in addition to NPCs that can respond to the microglial secretome for a more accurate representation.

Building on this idea only MGLs and NPCs were used in the study for simplicity, and the mechanism by which IL-6 confers risk for NDDs likely requires additional cell types. Campbell et al. (2014) identified cell types in the mouse brain responding to IL-6 via trans-signalling, predominantly in GFAP-positive astrocytes, Bergmann glia, lectin-bound microglia, and vascular endothelial cells, with scarce presence of IL-6 trans-signalling in neurons. Combining these rodent findings with our human-centric data implies that IL-6 trans-signalling to neural progenitor cells and neurons may not be the direct, central pathogenic mechanism in the CNS of both species and makes the case for the use of a more complex 3D model that contains additional relevant cell types when studying the effects of IL-6 on developing neurons. Moreover, while hiPSCs

provide a valuable model for studying human neurodevelopment within a human-relevant context at a molecular scale, they do not fully capture the complex interactions between additional higher-level systems seen in vivo, such as the peripheral immune system, placenta and blood brain barrier, which would be relevant in the context of this study (Zaretsky *et al.*, 2004; Campbell *et al.*, 2014; Crockett *et al.*, 2021; Li *et al.*, 2021, 2023; Bermick *et al.*, 2023). This is especially apparent since a recent MIA rodent model demonstrated IL-6 is not expected to pass through the placenta from the mother (Bermick *et al.*, 2023), even the IL-6 molecule can pass through human placental tissue (Zaretsky *et al.*, 2004). It is more likely that increased maternal prenatal IL-6 sets off a larger, pro-inflammatory chain reaction involving multiple cytokines, cell-types and tissues that subsequently in-directly increases IL-6 in the foetal brain. This limitation could be addressed by employing a multi-culture configuration, either in microglial-grafted organoids (Fagerlund *et al.*, 2022; Pașca *et al.*, 2022; Zhang *et al.*, 2022; Schafer *et al.*, 2023) or brain-on-a-chip fluidic systems (Liu *et al.*, 2020, 2022; Vila Cuenca *et al.*, 2021; Pașca *et al.*, 2022). These would offer viable methods to examine whether the release of sIL-6Ra, or other cytokines and chemokines from microglia in response to IL-6 can indeed have an impact on the NPC response, via additional cell types.

Third, after only 24h of IL-6 stimulation in co-culture, cytokine secretion by MGLs in response to IL-6 response might have been either too weak or short to activate relevant pathways in NPCs. The complexity of a chain of signalling pathways from additional cell types or physical cell connections over a more chronic period may be required, which in our *in vitro* setting may not entirely replicate. Our study suggests that a more prolonged cytokine exposure remains important to test in order to induce

substantial changes in NPCs, such as the 5-day exposure to brain organoids by Sarieva and colleagues (2023), given none were seen in response to the post IL-6 MGL-secreted microenvironment. Such extended exposure could more closely mimic the physiological conditions of a long-term prenatal infection, potentially offering a more realistic model for studying the effects of maternal immune activation on foetal brain development (Sarieva, Kagermeier, *et al.*, 2023).

Fourth, the noticeable presence of variation between different donor lines may mask detectable differences at an averaged donor level. Our sample size of N=4 donor lines, although in line with recommendations for the minimum sample size in such experiments (Dutan Polit *et al.*, 2023), coupled with the variability in responses generated by each individual donor may well constrain our ability to detect group-level differences. This is, however, consistent with the known heterogeneity of outcomes in response to maternal immune activation in humans and in rodent models, and that in most cases there is no negative outcome (Meyer, 2019; Mueller *et al.*, 2019). Therefore, the interaction between environment and genetic background needs to be considered, as evidenced by our findings of differential transcriptional response of NPCs from individuals with schizophrenia to IFN-gamma stimulation (Bhat *et al.*, 2022). Given the polygenic nature of NDDs and psychiatric disorders, we suggest hiPSC models that retain the genetic background of the donor are ideally placed to test this (Jansen et al., 2020; Singh et al., 2022; Trubetskoy et al., 2022). When conducting studies to examine the roles of cytokines on human neurodevelopment *in vitro* using healthy donor lines however, either greater statistical power, or stratification to allow selection of specific individuals to study are critical factors to consider when designing future studies. As such our data may be thought of as part of an iterative process to

refine the use of hiPSC models to study how cytokines influence neurodevelopment in health and disease states.

Despite the minimal impact of IL-6 stimulation on NPCs within our co-culture system there are clear and replicable effects of IL-6 on hiPSC-derived MGLs that are of relevance and open new avenues for research. For example, data from mice suggests that MIA accelerates the developmental programming of microglia, impairing their intended developmental functions (Matcovitch-Natan *et al.*, 2016). Our previous work demonstrated that the "MIA Poly I:C GD14 P0" module from Matcovitch-Natan et al. (2016) - a microglial gene set from newborn pups exposed to Poly I:C on gestational day 14 - was the most relevant module overlapping with our upregulated gene set in hiPSC-derived MGL monocultures exposed to IL-6 for 3h (Couch *et al.*, 2023). Additionally, a recent study that analysed transcriptomes and epigenetic profiles at various developmental stages in both foetal and postnatal human microglia has identified IL-6 as ligand of particular significance in predicting the postnatal microglial transcriptome, indicating that IL-6 may play a role in promoting the development of a mature, postnatal microglial phenotype (Han *et al.*, 2023). This raises the idea: Could the primary mechanism by which IL-6 increases NDD risk prenatally in offspring be via the alteration of typical developmental functions of microglia following IL-6 exposure? This guides several important questions unaddressed by the present study; (1) are the MGLs in this study are responding to IL-6 through cis- or trans-signalling (2) what causes the functional shift between these two signalling states, and (3) whether and how this signalling state transition operates in the CNS, all of which need to be addressed in future studies. Distinguishing these effects can be carried out in specific studies to block the IL-6 trans-signalling pathway in microglia using a soluble IL-6ST

compound and compare functional outcomes. Overall, these aspects represent a critical area for further investigation to understand the complex dynamics of neurodevelopmental changes under maternal immune activation and the influence of IL-6 on NDD risk.

In conclusion, our findings show that hiPSC-derived NPCs respond to IL-6 when sIL-6Ra is present, above a concentration of 1µg/ml, a level not met by hiPSC-derived MGLs from healthy donors *in vitro* and unchanged by acute IL-6 stimulation. Although these MGLs secrete a wide range of other cytokines and chemokines including TNF-α in response to IL-6, the proximal transcriptional and longer-term cellular effects on NPCs were minimal to absent. On the other hand, MGLs in co-culture showed robust transcriptional responses to IL-6 consistent with our prior observations and raising interesting new questions. Based on our observations we suggest that future studies seeking to develop *in vitro* hiPSC models to decipher the effects of IL-6 on human neurodevelopment should focus on incorporating microglia into more complex 3D models containing all relevant glial and neuronal cells that may respond to the microglia secretome. Such experiments should ideally be carried out on appropriate genetic risk backgrounds such as high polygenic risk for schizophrenia, which may reveal important disease-relevant mechanisms. Alternatively individual donors could be selected based on multivariate data from deeply-phenotype birth cohorts to identify cellular and molecular mechanisms associated with risk or resilience to IL-6 exposure during neurodevelopment.

Acknowledgements

The authors acknowledge use of King's Computational Research, Engineering and Technology Environment (CREATE) and are thankful to George Chennell of the Wohl Cellular Imaging Centre at King's College London for technical support during live imaging. ACMC, DPS and ACV acknowledge financial support for this study from the National Centre for the Replacement, Refinement and Reduction of Animals in Research (NC/S001506/1). RM and AB are in receipt of the MRC-Sackler Ph.D. Programme studentship as part of the MRC Centre for Neurodevelopmental Disorders (Medical Research Council MR/P502108/1).

Conflict of Interest

The authors declare no competing interests.

References

Adhya, D. *et al.* (2021) 'Atypical Neurogenesis in Induced Pluripotent Stem Cells From Autistic Individuals', *Biological Psychiatry*, 89(5), pp. 486–496. doi: 10.1016/j.biopsych.2020.06.014.

Allswede, D. M. *et al.* (2020) 'Cytokine concentrations throughout pregnancy and risk for psychosis in adult offspring: a longitudinal case-control study', *The Lancet Psychiatry*, 7(3), pp. 254–261. doi: 10.1016/S2215-0366(20)30006-7.

Arrode-Brusés, G. and Brusés, J. L. (2012) 'Maternal immune activation by poly(I:C) induces expression of cytokines IL-1β and IL-13, chemokine MCP-1 and colony stimulating factor VEGF in fetal mouse brain', *Journal of Neuroinflammation*, 9. doi: 10.1186/1742-2094-9-83.

Azuma, H. *et al.* (2000) 'Analysis of soluble interleukin 6 receptor in cerebprospinal fluid in inflammatory and non-inflammatory conditions', *Cytokine*, 12(2), pp. 160–164. doi: 10.1006/cyto.1999.0534.

De Bartolomeis, A. *et al.* (2014) 'Glutamatergic postsynaptic density protein dysfunctions in synaptic plasticity and dendritic spines morphology: Relevance to schizophrenia and other behavioral disorders pathophysiology, and implications for novel therapeutic approaches', *Molecular Neurobiology*, pp. 484–511. doi: 10.1007/s12035-013-8534-3.

Bayés, Á. *et al.* (2011) 'Characterization of the proteome, diseases and evolution of the human postsynaptic density', *Nature Neuroscience*, 14(1), pp. 19–21. doi: 10.1038/nn.2719.

Bennett, M. L. *et al.* (2016) 'New tools for studying microglia in the mouse and human CNS', *Proceedings of the National Academy of Sciences of the United States of America*, 113(12), pp. E1738–E1746. doi: 10.1073/pnas.1525528113.

Bermick, J. *et al.* (2023) 'The fetal response to maternal inflammation is dependent upon maternal IL-6 in a murine model', *Cytokine*, 167, p. 156210. doi: 10.1016/j.cyto.2023.156210.

Bhat, A. *et al.* (2022) 'Attenuated transcriptional response to pro-inflammatory cytokines in schizophrenia hiPSC-derived neural progenitor cells', *Brain, Behavior, and Immunity*, 105, pp. 82–97. doi: 10.1016/j.bbi.2022.06.010.

Bitanihirwe, B. K. Y. *et al.* (2009) 'Glutamatergic deficits and parvalbumin-containing inhibitory neurons in the prefrontal cortex in schizophrenia', *BMC Psychiatry*, 9. doi: 10.1186/1471-244X-9-71.

Campbell, I. L. *et al.* (2014) 'Trans-signaling is a dominant mechanism for the pathogenic actions of interleukin-6 in the brain', *Journal of Neuroscience*, 34(7), pp. 2503–2513. doi: 10.1523/JNEUROSCI.2830-13.2014.

Chehboun, S. *et al.* (2017) 'Epstein-Barr virus-induced gene 3 (EBI3) can mediate IL-6 trans-signaling', *Journal of Biological Chemistry*, 292(16), pp. 6644–6656. doi: 10.1074/jbc.M116.762021.

Chukaew, P. *et al.* (2022) 'Correlation of BDNF, VEGF, TNF-α, and S100B with cognitive impairments in chronic, medicated schizophrenia patients', *Neuropsychopharmacology Reports*, 42(3), pp. 281–287. doi: 10.1002/npr2.12261.

Couch, A. C. M. *et al.* (2023) 'Acute IL-6 exposure triggers canonical IL6Ra signaling in hiPSC microglia, but not neural progenitor cells', *Brain, Behavior, and Immunity*, 110, pp. 43–59. doi: 10.1016/j.bbi.2023.02.007.

Crockett, A. M. *et al.* (2021) 'Disruption of the blood-brain barrier in 22q11.2 deletion syndrome', *Brain*, 144(5), pp. 1351–1360. doi: 10.1093/brain/awab055.

Deans, P. J. M. *et al.* (2017) 'Psychosis Risk Candidate ZNF804A Localizes to Synapses and Regulates Neurite Formation and Dendritic Spine Structure', *Biological Psychiatry*, 82(1), pp. 49–61. doi: 10.1016/j.biopsych.2016.08.038.

Diemel, L. T., Jackson, S. J. and Cuzner, M. L. (2003) 'Role for TGF-β1, FGF-2 and PDGF-AA in A Myelination of CNS Aggregate Cultures Enriched with Macrophages', *Journal of Neuroscience Research*, 74(6), pp. 858–867. doi: 10.1002/jnr.10837.

Dobin, A. *et al.* (2013) 'STAR: Ultrafast universal RNA-seq aligner', *Bioinformatics*, 29(1), pp. 15–21. doi: 10.1093/bioinformatics/bts635.

Dráberová, E. *et al.* (2008) 'Class III β-tubulin is constitutively coexpressed with glial fibrillary acidic protein and nestin in midgestational human fetal astrocytes: Implications for phenotypic identity', *Journal of Neuropathology and Experimental Neurology*, 67(4), pp. 341–354. doi: 10.1097/NEN.0b013e31816a686d.

Dutan Polit, L. *et al.* (2023) 'Recommendations, guidelines, and best practice for the use of human induced pluripotent stem cells for neuropharmacological studies of neuropsychiatric disorders', *Neuroscience Applied*, 2, p. 101125. doi: 10.1016/J.NSA.2023.101125.

Eze, U. C. *et al.* (2021) 'Single-cell atlas of early human brain development highlights heterogeneity of human neuroepithelial cells and early radial glia', *Nature Neuroscience*, 24(4), pp. 584–594. doi: 10.1038/s41593-020-00794-1.

Fagerlund, I. *et al.* (2022) 'Microglia-like cells promote neuronal functions in cerebral organoids', *Cells*, 11(1). doi: 10.3390/cells11010124.

Ferreira, R. C. *et al.* (2013) 'Functional IL6R 358Ala allele impairs classical IL-6 receptor signaling and influences risk of diverse inflammatory diseases', *PLoS genetics*, 9(4). doi: 10.1371/JOURNAL.PGEN.1003444.

Glynn, M. W. and McAllister, A. K. (2006) 'Immunocytochemistry and quantification of protein colocalization in cultured neurons', *Nature Protocols*, 1(3), pp. 1287–1296. doi: 10.1038/nprot.2006.220.

Graham, A. M. *et al.* (2018) 'Maternal Systemic Interleukin-6 During Pregnancy Is Associated With Newborn Amygdala Phenotypes and Subsequent Behavior at 2 Years of Age', *Biological Psychiatry*, 83(2), pp. 109–119. doi: 10.1016/j.biopsych.2017.05.027.

Grunwald, L. M. *et al.* (2019) 'Comparative characterization of human induced pluripotent stem cells (hiPSC) derived from patients with schizophrenia and autism', *Translational Psychiatry*, 9(1). doi: 10.1038/s41398-019-0517-3.

Guidotti, A. *et al.* (2000) 'Decrease in reelin and glutamic acid decarboxylase67 (GAD67) expression in schizophrenia and bipolar disorder: A postmortem brain study', *Archives of General Psychiatry*, 57(11), pp. 1061–1069. doi: 10.1001/archpsyc.57.11.1061.

Haenseler, W. *et al.* (2017) 'A Highly Efficient Human Pluripotent Stem Cell Microglia Model Displays a Neuronal-Co-culture-Specific Expression Profile and Inflammatory Response', *Stem Cell Reports*, 8(6), pp. 1727–1742. doi: 10.1016/j.stemcr.2017.05.017.

Han, C. Z. *et al.* (2023) 'Human microglia maturation is underpinned by specific gene regulatory networks', *Immunity*, 56(9), pp. 2152-2171.e13. doi: 10.1016/j.immuni.2023.07.016.

Hashimoto, T. *et al.* (2008) 'Alterations in GABA-related transcriptome in the dorsolateral prefrontal cortex of subjects with schizophrenia', *Molecular Psychiatry*, 13(2), pp. 147–161. doi: 10.1038/sj.mp.4002011.

Hinks, G. L. and Franklin, R. J. M. (1999) 'Distinctive patterns of PDGF-A, FGF-2, IGF-I, and TGF-β1 gene expression during remyelination of experimentally-induced spinal cord demyelination', *Molecular and Cellular Neurosciences*, 14(2), pp. 153–168. doi: 10.1006/mcne.1999.0771.

Holloway, T. *et al.* (2013) 'Prenatal stress induces schizophrenia-like alterations of serotonin 2A and metabotropic glutamate 2 receptors in the adult offspring: Role of

maternal immune system', *Journal of Neuroscience*, 33(3), pp. 1088–1098. doi: 10.1523/JNEUROSCI.2331-12.2013.

Jansen, A. G. *et al.* (2020) 'Psychiatric Polygenic Risk Scores as Predictor for Attention Deficit/Hyperactivity Disorder and Autism Spectrum Disorder in a Clinical Child and Adolescent Sample', *Behavior Genetics*, 50(4), pp. 203–212. doi: 10.1007/s10519-019-09965-8.

Jao, J. and Ciernia, A. V. (2021) 'MGEnrichment: A web application for microglia gene list enrichment analysis', *PLoS Computational Biology*, 17(11), p. e1009160. doi: 10.1371/journal.pcbi.1009160.

Karolewicz, B. *et al.* (2010) 'Reduced level of glutamic acid decarboxylase-67 kDa in the prefrontal cortex in major depression', *International Journal of Neuropsychopharmacology*, 13(4), pp. 411–420. doi: 10.1017/S1461145709990587.

Kawahara, H. *et al.* (2008) 'Neural RNA-binding protein Musashi1 inhibits translation initiation by competing with eIF4G for PABP', *Journal of Cell Biology*, 181(4), pp. 639–653. doi: 10.1083/jcb.200708004.

Khandaker, G. M. *et al.* (2014) 'Association of serum interleukin 6 and C-reactive protein in childhood with depression and psychosis in young adult life a population-based longitudinal study', *JAMA Psychiatry*, 71(10), pp. 1121–1128. doi: 10.1001/jamapsychiatry.2014.1332.

Kuljis, D. A. *et al.* (2019) 'Fluorescence-based quantitative synapse analysis for cell type-specific connectomics', *eNeuro*, 6(5). doi: 10.1523/ENEURO.0193-19.2019.

Lee, S. *et al.* (2007) 'A Dual Role of Lipocalin 2 in the Apoptosis and Deramification of Activated Microglia', *The Journal of Immunology*, 179(5), pp. 3231–3241. doi: 10.4049/jimmunol.179.5.3231.

Li, H. *et al.* (2009) 'The Sequence Alignment/Map format and SAMtools', *Bioinformatics*, 25(16), pp. 2078–2079. doi: 10.1093/bioinformatics/btp352.

Li, Y. *et al.* (2021) 'Investigation of neurodevelopmental deficits of 22 q11.2 deletion syndrome with a patient-ipsc-derived blood–brain barrier model', *Cells*, 10(10). doi: 10.3390/cells10102576.

Li, Y. *et al.* (2023) 'Inhibition of Abl Kinase by Imatinib Can Rescue the Compromised Barrier Function of 22q11.2DS Patient-iPSC-Derived Blood–Brain Barriers', *Cells*, 12(3). doi: 10.3390/cells12030422.

Liao, Y. *et al.* (2019) 'WebGestalt 2019: gene set analysis toolkit with revamped UIs and APIs', *Nucleic Acids Research*, 47(W1), pp. W199–W205. doi: 10.1093/nar/gkz401.

Liao, Y., Smyth, G. K. and Shi, W. (2019) 'The R package Rsubread is easier, faster, cheaper and better for alignment and quantification of RNA sequencing reads', *Nucleic Acids Research*, 47(8), p. e47. doi: 10.1093/nar/gkz114.

Lin, J. *et al.* (2020) 'Neuroregenerative and protective functions of Leukemia Inhibitory Factor in perinatal hypoxic-ischemic brain injury', *Experimental Neurology*, 330. doi: 10.1016/j.expneurol.2020.113324.

Lionel, A. C. *et al.* (2013) 'Rare exonic deletions implicate the synaptic organizer gephyrin (GPHN) in risk for autism, schizophrenia and seizures', *Human Molecular Genetics*, 22(10), pp. 2055–2066. doi: 10.1093/hmg/ddt056.

Liu, L. *et al.* (2020) 'Three-dimensional brain-on-chip model using human iPSC-derived GABAergic neurons and astrocytes: Butyrylcholinesterase posttreatment for acute malathion exposure', *PLoS ONE*, 15(3). doi: 10.1371/journal.pone.0230335.

Liu, L. *et al.* (2022) 'A Three-Dimensional Brain-on-a-Chip Using Human iPSC-Derived GABAergic Neurons and Astrocytes', in *Methods in Molecular Biology*, pp. 117–128. doi: 10.1007/978-1-0716-2289-6_6.

Love, M. I., Huber, W. and Anders, S. (2014) 'Moderated estimation of fold change and dispersion for RNA-seq data with DESeq2', *Genome Biology*, 15(12), pp. 1–21. doi: 10.1186/s13059-014-0550-8.

Matcovitch-Natan, O. *et al.* (2016) 'Microglia development follows a stepwise program to regulate brain homeostasis', *Science*, 353(6301). doi: 10.1126/science.aad8670.

McGrath, E. L. *et al.* (2017) 'Differential Responses of Human Fetal Brain Neural Stem Cells to Zika Virus Infection', *Stem Cell Reports*, 8(3), pp. 715–727. doi: 10.1016/j.stemcr.2017.01.008.

Melief, J. *et al.* (2012) 'Phenotyping primary human microglia: Tight regulation of LPS responsiveness', *GLIA*, 60(10), pp. 1506–1517. doi: 10.1002/glia.22370.

Meyer, U. (2019) 'Neurodevelopmental Resilience and Susceptibility to Maternal Immune Activation', *Trends in Neurosciences*, 42(11), pp. 793–806. doi: 10.1016/j.tins.2019.08.001.

Mirabella, F. *et al.* (2021) 'Prenatal interleukin 6 elevation increases glutamatergic synapse density and disrupts hippocampal connectivity in offspring', *Immunity*, 54(11), pp. 2611-2631.e8. doi: 10.1016/j.immuni.2021.10.006.

Miyata, S. *et al.* (2021) 'Global knockdown of glutamate decarboxylase 67 elicits emotional abnormality in mice', *Molecular Brain*, 14(1). doi: 10.1186/s13041-020-00713-2.

Moghaddam, B. and Javitt, D. (2012) 'From revolution to evolution: The glutamate hypothesis of schizophrenia and its implication for treatment', *Neuropsychopharmacology*, 37(1), pp. 4–15. doi: 10.1038/npp.2011.181.

Mueller, F. S. *et al.* (2019) 'Influence of poly(I:C) variability on thermoregulation, immune responses and pregnancy outcomes in mouse models of maternal immune activation', *Brain, Behavior, and Immunity*, 80, pp. 406–418. doi: 10.1016/j.bbi.2019.04.019.

Nehme, R. *et al.* (2018) 'Combining NGN2 Programming with Developmental Patterning Generates Human Excitatory Neurons with NMDAR-Mediated Synaptic Transmission', *Cell reports*, 23(8), pp. 2509–2523. doi: 10.1016/J.CELREP.2018.04.066.

Nieland, T. J. F. *et al.* (2014) 'High Content Image Analysis Identifies Novel Regulators of Synaptogenesis in a High-Throughput RNAi Screen of Primary Neurons', *PLoS ONE*, 9(3), p. 91744. doi: 10.1371/JOURNAL.PONE.0091744.

Nowakowski, T. J. *et al.* (2017) 'Spatiotemporal gene expression trajectories reveal developmental hierarchies of the human cortex', *Science*, 358(6368), pp. 1318–1323. doi: 10.1126/science.aap8809.

Oni-Orisan, A. *et al.* (2008) 'Altered Vesicular Glutamate Transporter Expression in the Anterior Cingulate Cortex in Schizophrenia', *Biological Psychiatry*, 63(8), pp. 766–775. doi: 10.1016/j.biopsych.2007.10.020.

Onwordi, E. C. *et al.* (2020) 'Synaptic density marker SV2A is reduced in schizophrenia patients and unaffected by antipsychotics in rats', *Nature Communications*, 11(1), pp. 1–11. doi: 10.1038/s41467-019-14122-0.

Onwordi, E. C. *et al.* (2023) 'Synaptic Terminal Density Early in the Course of Schizophrenia: An In Vivo UCB-J Positron Emission Tomographic Imaging Study of Synaptic Vesicle Glycoprotein 2A', *Biological Psychiatry*, 0(0). doi: 10.1016/j.biopsych.2023.05.022.

Ozaki, K. *et al.* (2020) 'Maternal immune activation induces sustained changes in fetal microglia motility', *Scientific Reports*, 10(1), pp. 1–19. doi: 10.1038/s41598-020-78294-2.

Park, G. H. *et al.* (2020) 'Activated microglia cause metabolic disruptions in developmental cortical interneurons that persist in interneurons from individuals with schizophrenia', *Nature Neuroscience*, 23(11), pp. 1352–1364. doi: 10.1038/s41593-020-00724-1.

Pașca, S. P. *et al.* (2022) 'A nomenclature consensus for nervous system organoids and assembloids', *Nature*, 609(7929), pp. 907–910. doi: 10.1038/s41586-022-05219-6.

Potter, H. G. *et al.* (2023) 'Maternal behaviours and adult offspring behavioural deficits are predicted by maternal TNFα concentration in a rat model of neurodevelopmental disorders', *Brain, Behavior, and Immunity*, 108, pp. 162–175. doi: 10.1016/J.BBI.2022.12.003.

Rasmussen, J. M. *et al.* (2019) 'Maternal Interleukin-6 concentration during pregnancy is associated with variation in frontolimbic white matter and cognitive development in early life', *NeuroImage*, 185, pp. 825–835. doi: 10.1016/j.neuroimage.2018.04.020.

Reeh, H. *et al.* (2019) 'Response to IL-6 trans- A nd IL-6 classic signalling is determined by the ratio of the IL-6 receptor α to gp130 expression: Fusing experimental insights and dynamic modelling', *Cell Communication and Signaling*, 17(1), pp. 1–21. doi: 10.1186/s12964-019-0356-0.

Rose-John, S. (2001) 'Coordination of interleukin-6 biology by membrane bound and soluble receptors', in *Advances in Experimental Medicine and Biology*. Kluwer Academic/Plenum Publishers, pp. 145–151. doi: 10.1007/978-1-4615-0685-0_19.

Rose-John, S. *et al.* (2009) 'Interleukin-6 Trans-Signaling and Colonic Cancer Associated with Inflammatory Bowel Disease', *Current Pharmaceutical Design*, 15(18), pp. 2095–2103. doi: 10.2174/138161209788489140.

Rose-John, S. (2012) 'Il-6 trans-signaling via the soluble IL-6 receptor: Importance for the proinflammatory activities of IL-6', *International Journal of Biological Sciences*, 8(9), pp. 1237–1247. doi: 10.7150/ijbs.4989.

Rose-John, S. (2018) 'Interleukin-6 family cytokines', *Cold Spring Harbor Perspectives in Biology*, 10(2). doi: 10.1101/cshperspect.a028415.

Rudolph, M. D. *et al.* (2018) 'Maternal IL-6 during pregnancy can be estimated from newborn brain connectivity and predicts future working memory in offspring', *Nature Neuroscience*, 21(5), pp. 765–772. doi: 10.1038/s41593-018-0128-y.

Samuelsson, A. M. *et al.* (2006) 'Prenatal exposure to interleukin-6 results in inflammatory neurodegeneration in hippocampus with NMDA/GABAA dysregulation and impaired spatial learning', *American Journal of Physiology - Regulatory Integrative and Comparative Physiology*, 290(5), pp. 1345–1356. doi: 10.1152/ajpregu.00268.2005.

Sarieva, K., Kagermeier, T., *et al.* (2023) 'Human brain organoid model of maternal immune activation identifies radial glia cells as selectively vulnerable', *Molecular Psychiatry*, pp. 1–13. doi: 10.1038/s41380-023-01997-1.

Sarieva, K., Hildebrand, F., *et al.* (2023) 'Pluripotent stem cell-derived neural progenitor cells can be used to model effects of IL-6 on human neurodevelopment', *Disease Models & Mechanisms*, 16(11). doi: 10.1242/DMM.050306.

Schafer, S. T. *et al.* (2023) 'An in vivo neuroimmune organoid model to study human microglia phenotypes', *Cell*, 186(10), pp. 2111-2126.e20. doi: 10.1016/J.CELL.2023.04.022.

Scheller, J. *et al.* (2011) 'The pro- and anti-inflammatory properties of the cytokine interleukin-6', *Biochimica et Biophysica Acta - Molecular Cell Research*, 1813(5), pp. 878–888. doi: 10.1016/j.bbamcr.2011.01.034.

Shi, Y., Kirwan, P. and Livesey, F. J. (2012) 'Directed differentiation of human pluripotent stem cells to cerebral cortex neurons and neural networks', *Nature Protocols*, 7(10), pp. 1836–1846. doi: 10.1038/nprot.2012.116.

Shum, C. *et al.* (2015) 'Utilizing induced pluripotent stem cells (iPSCs) to understand the actions of estrogens in human neurons', *Hormones and Behavior*, 74, pp. 228–242. doi: 10.1016/J.YHBEH.2015.06.014.

Shum, C. *et al.* (2020) 'Δ9-tetrahydrocannabinol and 2-AG decreases neurite outgrowth and differentially affects ERK1/2 and Akt signaling in hiPSC-derived cortical neurons', *Molecular and Cellular Neuroscience*, 103. doi: 10.1016/j.mcn.2019.103463.

Singh, T. *et al.* (2022) 'Rare coding variants in ten genes confer substantial risk for schizophrenia', *Nature*, 604(7906), pp. 509–516. doi: 10.1038/s41586-022-04556-w.

Smith, S. E. P. *et al.* (2007) 'Maternal immune activation alters fetal brain development through interleukin-6', *Journal of Neuroscience*, 27(40), pp. 10695–10702. doi: 10.1523/JNEUROSCI.2178-07.2007.

Südhof, T. C. (2017) 'Synaptic Neurexin Complexes: A Molecular Code for the Logic of Neural Circuits', *Cell*. Cell, pp. 745–769. doi: 10.1016/j.cell.2017.10.024.

Trubetskoy, V. *et al.* (2022) 'Mapping genomic loci implicates genes and synaptic biology in schizophrenia', *Nature 2022 604:7906*, 604(7906), pp. 502–508. doi: 10.1038/s41586-022-04434-5.

Vila Cuenca, M. *et al.* (2021) 'Engineered 3D vessel-on-chip using hiPSC-derived endothelial- and vascular smooth muscle cells', *Stem Cell Reports*, 16(9), pp. 2159–2168. doi: 10.1016/j.stemcr.2021.08.003.

Warre-Cornish, K. *et al.* (2020) 'Interferon-γ signaling in human iPSC–derived neurons recapitulates neurodevelopmental disorder phenotypes', *Science Advances*, 6(34). doi: 10.1126/sciadv.aay9506.

van Wilgenburg, B. *et al.* (2013) 'Efficient, Long Term Production of Monocyte-Derived Macrophages from Human Pluripotent Stem Cells under Partly-Defined and Fully-Defined Conditions', *PLoS ONE*, 8(8). doi: 10.1371/journal.pone.0071098.

Wingett, S. W. and Andrews, S. (2018) 'FastQ Screen: A tool for multi-genome mapping and quality control', *F1000Research*, 7, p. 1338. doi: 10.12688/f1000research.15931.2.

Wolf, J., Rose-John, S. and Garbers, C. (2014) 'Interleukin-6 and its receptors: a highly regulated and dynamic system', *Cytokine*, 70(1), pp. 11–20. doi: 10.1016/j.cyto.2014.05.024.

Zaretsky, M. V. *et al.* (2004) 'Transfer of inflammatory cytokines across the placenta', *Obstetrics and Gynecology*, 103(3). doi: 10.1097/01.AOG.0000114980.40445.83.

Zhang, W. *et al.* (2022) 'Microglia-containing human brain organoids for the study of brain development and pathology', *Molecular Psychiatry*, pp. 1–12. doi: 10.1038/s41380-022-01892-1.

Zhang, Y. *et al.* (2016) 'Purification and Characterization of Progenitor and Mature Human Astrocytes Reveals Transcriptional and Functional Differences with Mouse', *Neuron*, 89(1), pp. 37–53. doi: 10.1016/j.neuron.2015.11.013.

Zhao, H. *et al.* (2018) 'FasL incapacitation alleviates CD4+ T cells-induced brain injury through remodeling of microglia polarization in mouse ischemic stroke', *Journal of Neuroimmunology*, 318, pp. 36–44. doi: 10.1016/j.jneuroim.2018.01.017.